Specific presynaptic functions require distinct Drosophila Ca_v2 splice isoforms

Christopher Bell*[1], Lukas Kilo*[2], Daniel Gottschalk[1], Hanna Kern[1], Jashar Arian[1], Lea Deneke[1], Oliver Kobler[3], Christof Rickert[1], Julia Strauß[1], Martin Heine[1], Carsten Duch[1], Stefanie Ryglewski[#1]

[1] Johannes Gutenberg University Mainz, Institute of Developmental Biology and Neurobiology, Biocenter 1, Hanns-Dieter Hüsch Weg 15, 55128 Mainz

[2] RWTH Aachen University, Lehrstuhl für Entwicklungsbiologie, Worringerweg 3, 52074 Aachen

[3] Leibniz Institute for Neurobiology Magdeburg, Combinatorial NeuroImaging Core Facility, Brenneckestraße 6, 39118 Magdeburg

* these authors contributed equally

[#] corresponding author

Abstract: 289 words

Introduction: 698 words

Results: 4634 words

Discussion: 1976 words

figures: 6

tables: 3

Abstract

The multiplicity of neural circuits that accommodate the sheer infinite number of computations conducted by brains requires diverse synapse and neuron types. At the vertebrate presynaptic active zone functional diversity can be achieved by the expression of different voltage gated calcium channels of the Ca_v2 family. In fact, release probability and other aspects of presynaptic function are tuned by different combinations of $Ca_v2.1$, $Ca_v2.2$, and $Ca_v2.3$ channels. By contrast, most invertebrate genomes contain only one Ca_v2 gene. The one *Drosophila* Ca_v2 homolog, cacophony, localizes to presynaptic active zones to induce synaptic vesicle release. We hypothesize that Drosophila Ca_v2 functional diversity is enhanced by two specific exon pairs that are mutually exclusively spliced and not conserved in vertebrates, one in the voltage sensor and one in the intracellular loop containing the binding site(s) for Caβ and G-protein βγ subunits. We test our hypothesis by combining opto- and electrophysiological with neuroanatomical approaches at a fast glutamatergic model synapse, the Drosophila larval neuromuscular junction. We find that alternative splicing in the voltage sensor affects channel activation voltage and is imperative for normal synapse function. Only the isoform with the higher activation voltage localizes to the presynaptic active zone and mediates evoked release. Removal of this Ca_v2 splice isoforms renders fast glutamatergic synapses non-functional. The By contrast, alternative splicing at the other alternative exon does not affect Ca_v2 presynaptic expression, but it tunes multiple aspects of presynaptic function. While expression of one exon yields normal transmission, expression of the other exon reduces channel number in the active zone and thus release probability. It also affects short term plasticity and abolishes presynaptic homeostatic plasticity. Thus, in *Drosophila* alternative splicing provides a mechanism to regulate different aspects of presynaptic functions with only one Ca_v2 gene.

Introduction

Information transfer at fast chemical synapses requires action potential triggered calcium influx through voltage gated calcium channels (VGCCs) into the presynaptic terminal, which in turn initiates synaptic vesicle (SV) release through a complex cascade of biophysical and biochemical reactions (Südhof 2013; 2014; Dittman, Ryan 2019). The millisecond temporal precision of SV release upon the arrival of an action potential in the axon terminal requires clustering of the VGCCs in a spatially restricted presynaptic specialization, named the presynaptic active zone (AZ; Eggermann et al. 2011; Südhof 2012; Van Vactor, Sigrist 2017; Dolphin, Lee 2020; Emperador-Melero, Kaeser 2020). At the AZ, protein-protein interactions ensure a nanoscale coupling of VGCCs to SVs in the readily releasable pool (Kittel et al. 2006), an arrangement that supports efficient and fast neurotransmission (Eggermann et al. 2011).

Despite these common organizational principles, fast chemical synapses are highly heterogeneous to accommodate the diverse computational requirements of different types of neurons and brain circuits (Moser et al. 2023; Zhang et al. 2022). One means of synapse diversification is to organize VGCCs heterogeneously at the AZ to modify either their nanoscale spatial relation to the SVs ready for release (Dittman, Ryan, 2019; Rebola et al. 2019), or the profiles of the calcium dynamics that shape release probability (P_r; Zhang et al. 2022). The calcium dynamics in nano- or microdomains are affected by VGCC number, clustering, and properties, and are thus strongly dependent on calcium channel subtype.

The vertebrate genome contains 10 genes encoding the α_1-subunit of VGCCs that fall into three families (Ca_v1, Ca_v2, Ca_v3; Dolphin, 2009). With the exception of Ca_v1 triggering release at retinal ribbon and auditory brain stem synapses (Moser et al. 2020), Ca_v2 usually mediates evoked release at other mammalian synapses. The three subtypes of Ca_v2 exhibit different biophysical properties (Sheng et al. 2012), which may explain their different contribution to SV release at a given synapse (Li et al. 2007). $Ca_v2.1$ and $Ca_v2.2$ trigger SV release at most synapses and $Ca_v2.3$ likely make only a small contribution (Dietrich et al. 2003). However, all three Ca_v2 subtypes may co-localize to the same synapse and contribute to SV release (Takahashi, Momiyama 1993; Wheeler et al. 1994; Wu et al. 1998), and different types of mammalian synapses can utilize either only one subtype or combinations of Ca_v2 subtypes (reviewed in Zhang et al. 2022).

The Drosophila genome contains only 3 genes encoding α_1-subunits of VGCCs, each one homologous to one vertebrate Ca_v family (Littleton, Genetzky 2000). Therefore, the joint functions of mammalian $Ca_v2.1$, $Ca_v2.2$, and $Ca_v2.3$ are covered by only one Drosophila gene, namely *Dmca1A* (also named *cacophony* or *nightblindA*, Smith et al. 1996; 1998). Cacophony (cac) is, in fact, essential for fast synaptic transmission in Drosophila (Kawasaki et al. 2002) and loss of cac cannot be compensated for by the Drosophila counterparts of Ca_v1 or Ca_v3 (Krick et al. 2021). This suggests that Drosophila lacks the combinatorial logic of employing different blends of $Ca_v2.1$, $Ca_v2.2$, and $Ca_v2.3$ for fine-tuning of P_r as present in mammals. However, the Drosophila *Ca_v2* locus contains two mutually exclusive alternative splice sites that are not present in the vertebrate *Ca_v2* gene family, one in the voltage sensor in the fourth transmembrane domain of the first homologous repeat (IS4) and one in the intracellular linker between the first and the second homologous repeats (I-II). Alternative splicing at these mutually exclusive sites may provide mechanisms to fine tune action potential triggered calcium dynamics at presynaptic active zones by adjusting the numbers, nanoscale localization and properties of presynaptic Ca_v2 VGCCs. We test this hypothesis by employing the CRISPR-Cas9 technology to remove mutually exclusive exons at either the *IS4* or the *I-II* site and test the resulting functional consequences at the

Drosophila neuromuscular junction (NMJ), a well-established model for presynaptic function of a fast glutamatergic synapse (Adwood, Karunanithi 2002; Harris, Littleton 2015).

We find that alternative splicing at the *IS4* site affects Ca_v2 voltage activation and only one of both mutually exclusive splice events allows for presynaptic AZ localization and thus evoked synaptic transmission at a fast glutamatergic synapse. By contrast, alternative splicing at the *I-II* site does not affect presynaptic AZ localization, but it affects P_r, short term plasticity, and presynaptic homeostatic plasticity.

Results

The Drosophila *Ca_v2* homolog *cacophony* is located on the X-chromosome and contains multiple alternative splice sites but only 2 that are mutually exclusive (Fig. 1A). The first one is located in the fourth transmembrane domain of the first homologous repeat (IS4), and thus affects the voltage sensor. Both alternative *IS4* exons are 99 bp long and encode 33 amino acids (AAs). The polypeptide encoded by *IS4A* (first alternative exon of the *IS4* locus) differs from that of *IS4B* in 13 AAs and contains one more positively charged AA. The second mutually exclusive exon pair encodes part of the intracellular linker between homologous repeats I and II (*I-II*; Fig. 1A), and thus affects binding sites for calcium channel β subunits (Ca_β) and G-protein βγ subunits ($G_{\beta\gamma}$). Both alternative *I-II* exons are 117 bp long and encode 39 AAs. The polypeptide encoded by *I-IIA* (first alternative exon of the *I-II* locus) differs from that of *I-IIB* in 23 AAs, which results in a predicted lack of the $G_{\beta\gamma}$ binding site and a less conserved α-subunit interaction domain (AID), the binding motif for Ca_β to the pore-forming α-subunit (Smith et al. 1998). We employ CRISPR-Cas9 to excise one of both alternative exons either at the *IS4* or the *I-II* loci (Fig. 1B). Genomic removal of *IS4A* results in fly strains that contain only the *IS4B* exon and are named *ΔIS4A* (Fig. 1B). Accordingly, genomic removal of the *I-IIA* exon results in flies with *I-IIB* only that are named *ΔI-IIA* (Fig. 1B). To analyze the functions of mutually exclusive exon variants, we create exon-out fly strains with removal of one exon at a time of each of the four exons (*IS4A*, *IS4B*, *I-IIA*, *I-IIB*). Excision of the respective exon is always confirmed by sequencing (see methods). Fly strains with first chromosomes that carry exon excisions are cantonized by 10 generations of backcrossing into CantonS wildtype flies. Exon-out strains are produced from either wildtype (CantonS) or white mutant flies (w^{1118}, see methods) as well as from fly strains with previously introduced N-terminal fluorophore tagging of the *Ca_v2* gene. Neither on-locus super folder GFP (sfGFP) tagging (Gratz et al. 2019), nor on-locus tagging of the endogenous cacophony channel with mEOS4b (Ghelani et al. 2023) impairs Ca_v2 localization at presynaptic active zones or synaptic function at the larval Drosophila NMJ. In this study, sfGFP-tagged (Fig. 1A) exon-variants serve analysis of channel localization and mEOS4b tagged (Fig. 1A) ones serve to count channel number in active zones, and untagged fly strains serve to control for possible effects of the fluorescent tags.

Of the 18 annotated *Ca_v2* transcripts in Drosophila, 13 remain upon removal of *IS4A*, 5 upon removal of *IS4B*, 8 upon removal of *I-IIA*, and 10 upon removal of *I-IIB* (Fig. 1C). For each mutually exclusive exon, we have created multiple exon-out fly strains. Each exon removal induces reproducible phenotypes (see methods). Removal of *IS4B* is embryonic lethal as confirmed in all CRISPR-Cas9 mediated excisions (n=12), both before and after crossing out into a wildtype background. Removal of each of the three other mutually exclusive exons results in viable fly strains, Drosophila larvae without any obvious deficits, before and after crossing out into a wildtype background, but with distinct behavioral phenotypes in adult flies (the latter are not further addressed in this study). Western blots with GFP tagged Ca_v2 channels test whether the channel protein is expressed in the CNS of all exon-out fly strains (Fig. 1D). For Western blot analysis, *ΔIS4B* flies are homozygous lethal and are thus used heterozygously over untagged wildtype channels that contain all exons. Brain homogenate from sfGFP tagged controls and from all exon-out fly strains with sfGFP tagged Ca_v2 channels yield a band at roughly the expected size of 250-270 kDa (Drosophila Ca_v2 isoforms range from 212 to 242 kDa and sfGFP is 27 kDa), whereas no band is detected in control brains without tagged Ca_v2 (Fig. 1D, right lane). Protein level in *ΔIS4B* flies (first band from left, Fig. 1D) is lower as compared to heterozygous controls with all isoforms (second band from left, Fig. 1D). Similarly, protein level in *ΔI-IIB* flies (fifth band from left, Fig. 1D) is lower as compared to homozygous controls with all isoforms (third and eighth band

from left, Fig. 1D), thus indicating that Ca_v2 isoform containing IS4B and I-IIB are normally abundantly expressed. By contrast, homozygous removal of *IS4A* or of *I-IIA* does not cause obvious differences in expression levels as compared to homozygous sfGFP tagged controls (Fig. 1D). Taken together, CRISPR-Cas9 is successfully employed to produce all possible distinct exon excisions at the mutually exclusive splice sites of the Drosophila *Ca_v2* homolog *cacophony* (*cac*). This now allows for analysis of *Ca_v2* exon specific functions.

We next analyze the functional consequences of the removal of each of the mutually exclusive exons at the *IS4* and at the *I-II* loci for Ca_v2 channel localization, channel number, and channel function at motoneuron presynaptic terminals of the larval Drosophila neuromuscular junction (NMJ).

IS4B localizes to presynaptic active zones and is required for evoked synaptic transmission

Drosophila Ca_v2 channels interact with the scaffold protein bruchpilot (brp) to localize to presynaptic active zones (Kittel et al. 2006; Ghelani et al. 2023). Immunohistochemical triple labels at the larval Drosophila NMJ test whether either one of the mutually exclusive exons at the *IS4* locus is required for correct presynaptic Ca_v2 localization. Motoneuron axon terminals on larval muscles 6 and 7 (M6/7) are labeled with HRP (Fig 2A-C, right row, blue), Ca_v2^{sfGFP} by α-GFP immunolabel (Figs. 2A-C, left row, green), and active zones by α-brp immunohistochemistry (Figs. 2A-C, second row, magenta). In controls, Ca_v2^{sfGFP} channels with full isoform diversity strictly co-localize with brp in presynaptic active zones (Fig. 2A) as previously reported (Gratz et al. 2019). The same is the case for Ca_v2 channels that contain IS4B but lack IS4A (ΔIS4A, Fig. 2B). By contrast, Ca_v2 channels that contain IS4A but lack IS4B (ΔIS4B) do not show strict active zone localization (Fig. 2C). Since *ΔIS4B* is homozygous lethal, heterozygous animals are used for triple labels of tagged ΔIS4B channels, the active zone marker brp, and motoneuron terminals on M6/7. Axon terminal shape and brp label in active zones are qualitatively normal, but the label for $Ca_v2^{\Delta IS4B}$ channels is weak and not restricted to active zones (Fig. 2C, white arrowheads). These data indicate that the *IS4B* exon might be required for targeting/localizing Ca_v2 channels within the active zone.

It has previously been shown that presynaptic Ca_v2 are required for normal evoked synaptic transmission at the Drosophila NMJ (Kawasaki et al. 2002). The reduced Ca_v2 label in presynaptic active zones goes along with reduced synaptic transmission (Kittel et al. 2006), whereas increased Ca_v2 channel numbers during presynaptic homeostatic plasticity are effective to increase mean quantal content (Ghelani et al. 2023). If Ca_v2 presynaptic active zone localization requires *IS4B* but not the *IS4A* exon, removal of *IS4B* but not *IS4A* should impair evoked synaptic transmission. Two electrode voltage clamp recordings from larval muscle 6 in abdominal segment 3 indicate that excitatory postsynaptic currents (EPSCs) as evoked by single presynaptic action potentials are similar in wildtype (CantonS, Fig. 2D, blue trace) and in animals with sfGFP tagged Ca_v2 channels (Fig. 2D, green trace). Upon removal of *IS4A*, EPSC amplitude is slightly but not significantly increased (Fig. 2D, ΔIS4A, orange trace, Fig. 2E orange). In transheterozygous animals (*ΔIS4B/ΔIS4A*) with removal of *IS4A* on one chromosome and *IS4B* on the other, EPSC amplitude is significantly reduced (Fig. 2D, black trace, Fig. 2E, black). Spontaneous synaptic vesicle (SV) release as characterized by the amplitude (Fig. 2F) and the frequency (Fig. 2G) of miniature postsynaptic currents (mPSCs) is not affected in *ΔIS4B/ΔIS4A* transheterozygotes. Together, these data indicate that *IS4A* is neither required for active zone localization of channels, nor for evoked synaptic transmission, whereas *IS4B* is required for normal active zone localization and synaptic transmission.

A limitation of these experiments is that homozygous removal of *IS4B* is embryonic lethal, so that presynaptic terminals that are devoid of Ca_v2 with the IS4B exon can only be studied in mosaic animals that are heterozygous for *IS4B* excision at most synapses but hemizygous *ΔIS4B* at few synapses of interest. Employing the FlpStop method (see methods, Fisher et al. 2017), mosaic animals with motoneurons to muscle 12 (M12) that are $\Delta IS4B/Ca_v2^{null}$ can be produced in otherwise heterozygous animals ($\Delta IS4B/Ca_v2$; Fig. 2H). In control animals, Ca_v2^{sfGFP} channels localize to brp positive active zones in motoneuron axon terminals on M12 (Fig. 2H, top row). By contrast, $Ca_v2^{\Delta IS4B}$ do not localize to brp positive active zones in motoneuron axon terminals on M12 (Fig. 2H, bottom row). Therefore, *IS4B* is indeed required for Ca_v2 active zone localization in excitatory glutamatergic axon terminals at the Drosophila NMJ. Consequently, evoked synaptic transmission is nearly abolished in motoneuron terminals that lack IS4B (Fig. 2I). We conclude that *IS4B* is required for evoked synaptic transmission from chemical presynaptic terminals, whereas *IS4A* has no essential function for action potential induced neurotransmitter release from presynaptic terminals.

The IS4B exon is required for sustained HVA Ca_v2 calcium current.

Technical constraints prohibit a voltage clamp characterization of IS4B containing Ca_v2 channels at the larval motoneuron presynaptic terminal, and the somatodendritic calcium current in larval motoneurons is mediated by the Drosophila Ca_v1 homolog *DmCa1D* (Worrell, Levine 2008; Kadas et al. 2017). However, Drosophila Ca_v2 currents have previously been shown in somatodendritic voltage clamp recordings from pupal and adult motoneuron somata (Ryglewski et al. 2012; 2014a; b). Although these recordings are not representative for Ca_v2 currents at larval presynaptic terminals, they show that Drosophila Ca_v2 channels can in principle contribute to transient and sustained as well as high (HVA) and low (LVA) voltage activated currents. Given that mutually exclusive splicing at the *IS4* site affects the voltage sensor (Fig. 1A) and that only the *IS4B* exon is required for evoked synaptic transmission, we next tested whether *IS4B* makes a significant contribution to a specific sub-type of Ca_v2 mediated calcium current. The comparison of voltage clamp recordings from adult flight motoneuron somata in animals with full Ca_v2 isoform diversity and mosaic animals with *IS4B* excision in only these motoneurons (see methods) shows that *IS4B* is required for sustained HVA Ca_v2 current. Following electrical inactivation of LVA currents with prepulses to -50 mV (Fig. 2J, left), HVA with an activation voltage of ~-30 mV shows a sustained component that is reliably recorded with full Ca_v2 isoform diversity (Fig. 2J, left current traces and IV diagram) but nearly absent in *ΔIS4B* motoneurons (Fig. 2J, right current traces and IV diagram). Therefore, the *IS4B* exon that is vital for evoked synaptic transmission promotes sustained HVA calcium current.

Alternative splicing at the I-II site does not affect active zone localization but channel number and release probability

Immunohistochemical triple label at the larval Drosophila NMJ tests whether either one of the mutually exclusive exons at the *I-II* locus is required for correct presynaptic Ca_v2 localization. Motoneuron axon terminals on larval muscles 6 and 7 (M6/7) are labeled with HRP (Fig. 3A-C, right column, blue), sfGFP tagged Ca_v2 channels by α-GFP immunolabel (Fig. 3A-C, left column, green), and active zones by α-brp immunocytochemistry (Fig. 2A-C, second column, magenta). In controls, sfGFP tagged Ca_v2 channels with full isoform diversity strictly co-localize with brp in presynaptic active zones (Fig. 3A) as also shown above (Fig. 2A). The same is the case for both mutually exclusive variants at the *I-II* locus. Ca_v2 channels that contain I-IIB but lack I-IIA ($Ca_v2^{\Delta I\text{-}IIA}$, Fig. 3B), and *vice versa*, Ca_v2 channels that contain I-IIA but

lack I-IIB (ΔI-IIB, Fig. 3C) show strict active zone localization (see overlays of brp and cac^{sfGFP} in Fig. 3B, C, third column). For all Ca_v2 isoforms that are targeted to the presynaptic active zones, quantification reveals similar Pearson co-localization coefficients of ~0.65 (Fig. 3D), which corresponds to previous reports (Krick et al. 2021). Moreover, the Manders 1 and 2 co-localization coefficients are similar for control, $Ca_v2^{\Delta IS4A}$, and both I-II locus isoforms $Ca_v2^{\Delta I\text{-}IIA}$ and $Ca_v2^{\Delta I\text{-}IIB}$ (Figs. 3E, F). In sum, alternative splicing at the *I-II* site does not affect Ca_v2 expression in presynaptic active zones.

However, removal of the *I-IIB* exon reduces the intensity of Ca_v2 immunolabel in active zones as compared to control or *ΔI-IIA* highly significantly by ~50% (Fig. 3H). These data indicate that *I-IIB* excision may result in fewer Ca_v2 channels per presynaptic active zone. We employ two electrode voltage clamp recordings from the postsynaptic cell (M6) to test for the resulting consequences on synaptic transmission (Figs. 3I-L). As shown above, the amplitude of the postsynaptic current (PSC) as evoked by an action potential in the presynaptic motor axon is similar in Canton S with untagged Ca_v2 and animals expressing Ca_v2^{sfGFP} channels (Fig. 2D). Removal of the *I-IIA* exon (*ΔI-IIA*, Fig. 3I, purple trace) does not result in significant differences of PSC amplitude as compared to tagged or untagged controls (Figs. 3I, J). By contrast, removal of the *I-IIB* exon (*ΔI-IIB*, Fig. 3I, orange trace) results in a reduction in PSC amplitude by ~50% (Fig. 3J), which matches the reduced channel immunofluorescence signal in active zones (Fig. 3H).

It seems unlikely that presynaptic Ca_v2 channel isoform type affects postsynaptic glutamate receptor type, numbers, or properties, because the amplitude of miniature postsynaptic currents (mPSCs) that result from spontaneous SV release does not differ between controls and animals with Ca_v2 exon excision (Fig. 3K). Similarly, it is unlikely that presynaptic Ca_v2 channel isoform type affects the size of the readily releasable pool of SVs because mPSC frequency is unaltered (Fig. 3L). In sum, these data show that neither exon at the *I-II* locus is required for Ca_v2 localization to active zones, but *I-IIB* is required for normal evoked synaptic transmission amplitude. A reduced amplitude of evoked synaptic transmission along with less intensive presynaptic Ca_v2 immunolabel in *ΔI-IIB* animals (Fig. 3H, J) is indicative for fewer calcium channels in active zones. Alternatively, the nanoscale localization of Ca_v2 could be affected by alternative splicing.

We assess the latter by dual color STED microscopy of the active zone marker brp and Ca_v2^{sfGFP} in different exon excision mutants (Figs. 4A-E). Collecting STED image stacks of synaptic boutons on muscle 6 (Fig. 4A) reveals numerous active zones in various spatial orientations relative to the focal plane (Fig. 4A-C). In a strict top view (Fig. 4C1) the central Ca_v2 cluster (magenta) is surrounded by four brp puncta (green). If the active zone lies tilted relative to the focal plane, the same arrangement is viewed from different angles (side views, Figs. 4C2-6). The localization of Ca_v2 relative to brp in different exon-out variants (Figs. 4D, E) is quantified by measuring the distance between the center of the Ca_v2 cluster and the center of the nearest brp punctum in top and side views within the same optical sections (see methods). In all Ca_v2 exon-out variants that are expressed in active zones (control, *ΔIS4A*, *ΔI-IIA* and *ΔI-IIB* but not *ΔIS4B*) the median distance ranges between 103 and 109 nm and reveals no significant differences (Kruskal-Wallis test, $p = 0.62$) between control (median distance, 106.1 nm) and any of the exon-out variants shown *(ΔIS4A*, *ΔI-IIA* and *ΔI-IIB*, Fig. 4E). Alternative splicing at the *I-II* locus does therefore neither affect targeting of Ca_v2 to active zones (Figs. 3A-F), nor Ca_v2 localization within the brp scaffold of the active zone (Figs. 4A-E).

This leaves changes in Ca_v2 properties or channel number in actives zones as plausible causes for the reduction in evoked synaptic transmission upon removal of the *I-IIB* exon (Figs. 3I, J). As previously

reported, channel number in presynaptic active zones can be estimated by live sptPALM imaging of mEOS4b tagged Ca_v2 channels at the NMJ (Ca_v2^{mEOS4b}, Ghelani et al. 2023). To estimate channel number in AZs of axon terminals on larval muscle M6 in controls, *ΔI-IIA*, and *ΔI-IIB* (Fig. 4F), the bleaching behavior of Ca_v2^{mEOS4b} signals in individual AZs is imaged during steady illumination. Discrete bleaching steps (Fig. 4G, dotted lines) indicate bleaching events of individual Ca_v2^{mEOS4b} molecules, and thus the fluorescence intensity of a single Ca_v2^{mEOS4b} channel. Larger channel numbers produce integer multiple fluorescence intensity amplitudes. Dividing the full fluorescence amplitude that is measured at the illumination onset of all channels in the active zone by the fluorescence intensity from a single channel yields total channel number per active zone. Quantification from three animals per genotype with at least 30 active zones per animal confirms a previous study (Ghelani et al. 2023) showing that control animals with full Ca_v2 channel isoform diversity express ~10 Ca_v2 channels per AZ (Fig. 4F, green, 10.8 ± 2 channels). Removing the alternative exon *I-IIA* does not affect channel number per active zone (Fig. 4F, purple, 10.5 ± 2 channels), but excision of *I-IIB* reduces channel number to ~ 50 % (Fig. 4F, orange, 5.6 ± 1 channels). A ~50% reduction in channel number counts in AZs (Fig. 4F) is in line with ~50 % reduction in Ca_v2 immunofluorescence in AZs (Fig. 3H) and evoked synaptic transmission (Figs. 3I, J) upon excision of *I-IIB*. In sum, these data indicate that the reduction of evoked synaptic transmission amplitude in *ΔI-IIB* is a consequence of reduced channel number.

Functional consequences of I-II site alternative splicing during repetitive firing

In addition to reducing the numbers of SVs that are released upon one presynaptic action potential (quantal content), removal of the *I-IIB* exon has significant effects on synaptic transmission during repetitive stimulation and on synaptic plasticity. First, the paired pulse ratio (PPR) is affected. In 0.5 mM calcium, controls with sfGFP-tagged Ca_v2 channels show slight paired pulse (PP) depression at interpulse interval (IPI) durations below 20 ms (Fig. 5A). Similarly, upon removal of the *I-IIA* exon (*ΔI-IIA*^{sfGFP}) PP depression is observed for IPIs below 20 ms (Fig. 5B). By contrast, upon removal of the *I-IIB* exon, some animals show PP depression and others PP facilitation, so that the average PPR is close to 1 for all IPIs, but the variance is large, in particular for short IPIs (Fig. 5C). In fact, for all IPIs the coefficient of variation reveals ~ 5-10 % variability of PPR across animals for control and for excision of *I-IIA* (Fig. 5D). By contrast, upon excision of ,*I-IIB* the variability for short IPIs is about 20 % (Fig. 5D).

Moreover, the time course and the variability of synaptic depression are affected by removal of the *I-IIB* exon. In 0.5 mM external calcium, repetitive stimulation of the NMJ to muscle M6/7 at 1 Hz frequency for 1 minute causes synaptic depression that reaches steady state at about 80 % of the initial transmission amplitude with a time constant of about 5 ms (Krick et al. 2021). The same is observed for Ca_v2^{sfGFP} controls (Figs. 5E, H) and upon removal of *I-IIA* (Figs 5F., H). Removal of *I-IIB* does not affect the magnitude of depression at 1 Hz stimulation (Fig. 5G), but it strongly increases the variability of transmission amplitude (Fig. 5G) and it significantly increases the time constant until steady state depression is reached (Fig. 5H). Similarly, removal of *I-IIA* does not affect the time course or amplitude of synaptic depression at 10 Hz stimulation (Figs. 5I, J, L), whereas excision of *I-IIB* significantly increases the time constant until steady state depression is reached (Fig. 5L), it slightly decreases the mean steady state depression amplitude (Fig. 5K), and it increases variability (see large standard error in Fig. 5K). Therefore, removal of *I-IIB* does not only cause fewer Ca_v2 channels in presynaptic active zones and a concomitant reduction of the amplitude of evoked synaptic transmission, it also strongly reduces the

reliability of PPRs at short IPIs and it significantly increases the variability of synaptic depression during repetitive stimulation.

However, motoneuron firing frequencies as previously measured during tethered crawling (Kadas et al. 2017) reach ~120 Hz during bursts of about 200 ms duration. Given that the main function of excitatory synaptic transmission to larval muscles is locomotion, it seems important to test stimulation protocols that reflect behaviorally relevant motoneuron firing patterns. Applying motoneuron stimulation for 200 ms duration at either 60 (Fig. 5M) or 120 Hz frequency (Fig. 5N) in 0.5 mM external Ca^{2+} reveals summation of the PSCs in control animals with GFP-tagged Ca_v2 channels (Figs. 5M, N, upper traces) as well as in animals without the *I-IIB* exon (*ΔI-IIB*, Figs. 5M, N, bottom traces). By contrast, upon excision of *I-IIA*, summation of PSCs is absent at 60 Hz but present at 120 Hz stimulation frequency (*ΔI-IIA*, Figs. 5M, N, middle traces). The reason why PSP summation occurs only at very high motoneuron firing frequencies (120 Hz) in *ΔI-IIA*, but already at 60 Hz in controls and in *ΔI-IIB* animals is a significantly smaller PSP half-width upon excision of the *I-IIA* exon (Fig. 5Q). This might be an indication for an effect of alternative *I-II* exon splicing on Ca_v2 channel biophysical properties (see discussion). The reduced PSC amplitudes in *ΔI-IIB* animals as compared to control and *ΔI-IIA* (Figs. 2I, J and Figs. 5A-N), and the reduced PSC half width in *ΔI-IIA* animals as compared to control and *ΔI-IIB* (Fig. 5Q) combine to different charge transfer courses during high frequency stimulation (Figs. 5M-P). We measure charge transfer as the total area under the postsynaptic response traces during 200 ms long stimulation bursts at either 60 Hz (Figs. 5M, O) or 120 Hz (Figs. 5N, P). The slightly higher single PSC amplitude of *ΔI-IIA* as compared to control (compared first PSCs in Figs. 5AB, EF, IJ, M, N) is compensated for by a smaller PSC half width (Fig. 5Q) so that total charge transfer during 200 ms duration bursts shows no significant differences in control versus *ΔI-IIA* animals, neither for 60 Hz (Fig. 5O) nor for 120 Hz (Fig. 5P). By contrast, as is the case for single evoked PSC amplitude, total charge transfer is significantly reduced upon removal of the *I-IIB* exon, both for 60 Hz stimulation (Fig. 5O) and for 120 Hz stimulation (Fig. 5P).

Although crawling speed of Drosophila larvae is mainly adjusted by varying the duration between subsequent peristaltic waves of motoneuron bursting (peristaltic wave period duration, Liu et al. 2023), differences in Ca_v2 mediated neuromuscular synaptic transmission may also play an important role. In accordance with reduced charge transfer to the postsynaptic muscle cell upon excision of the *I-IIB* exon (Figs. 5M-P), mean crawling speed is significantly reduced in *ΔI-IIB* animals (Fig. 5R). The mean crawling speed (including stops) of Ca_v2^{sfGFP} control larvae is roughly 0.2 mm per second and not significantly affected in transheterozygous *ΔI-IIA* over *ΔI-IIB* larvae that contain full Ca_v2 isoform diversity (Fig. 5A). Removal of *I-IIB* (*ΔI-IIB*) causes a significant decrease in mean locomotion speed (Fig. 5R, orange) whereas removal of *I-IIA* significantly increases speed (*ΔI-IIA*, Fig. 5R purple). Alterations in locomotion speed upon alternative Ca_v2 exon removal could either be caused by changes in mean ground speed (mean speed excluding stops), or by changes in the duration of stopping, or by both. Mean ground speed in controls is about 0.5 mm per second (Fig. 5S), which is slightly slower but within the range previously reported (0.65-0.8 mm per second, Wang et al. 1997; Guo et al. 2016). The decreased net locomotion speed in *ΔI-IIB* larvae is caused by significant reductions in the mean ground speed (Fig. 5S) paired with significant increases in the duration of stopping (Fig. 5T). By contrast, the net locomotion speed increase as observed in *ΔI-IIA* larvae is caused by significant increases in the mean ground speed (Fig. 5S) without significant changes in the duration of stopping (Fig. 5T). However, the maximum locomotion speed observed does not differ significantly between controls and any of the test groups (Kruskal Wallis test, p=0.14; Fig. 5U), although *ΔI-IIB* neuromuscular junctions show significantly

reduced charge transfer at 120 Hz motoneuron bursting (Fig. 5P). This may indicate a safety plateau of charge transfer at maximum speed.

I-IIB is required for presynaptic homeostatic plasticity

Chemical synapses are subject to various forms of short-term (Fioravante, Regehr 2011), Hebbian (Nicoll, Schmitz 2005) and homeostatic plastic adjustments (Turrigiano 2008). The Drosophila larval NMJ has become a prominent model to analyze the mechanisms underlying presynaptic homeostatic potentiation (PHP, Davis, Müller 2015). PHP is a compensatory increase in the number of SVs that are released upon one presynaptic action potential (quantal content) in response to reduced postsynaptic receptor function. Consequently, PSC amplitude is restored to its original setpoint despite reduced mPSC amplitudes. Quantal content can be increased by a larger size of the readily releasable pool (RRP) of SVs, or by elevated release probability (P_r). A recent study has shown that the induction of PHP at the Drosophila NMJ requires an increase in P_r that is mediated by increasing the number of Ca_v2 channels in the presynaptic active zone (from ~10 to ~12, Ghelani et al, 2023). Our data show that exclusion of *IS4B* impairs Ca_v2 localization to the AZ (Figs. 2H, I), whereas exclusion of *I-IIB* reduces Ca_v2 number in the presynaptic AZ (Fig. 4F), raising the question whether homeostatic plasticity is affected by *I-II* exon splicing. Acute pharmacological blockade of postsynaptic glutamate receptors with the bee wolf toxin, philanthotoxin (PhTx), is a well-established means to induce PHP within minutes at the Drosophila larval NMJ (Davis, Müller 2015; Ghelani et al. 2023). In control animals with GFP-tagged Ca_v2 channels as well as upon excision of the *I-IIA* exon (normal channel numbers, Fig. 4F), bath application of PhTx reliably reduces the amplitude of spontaneously occurring minis (mPSCs; control: Figs. 6A, B red; ΔI-IIA: Figs. 6E, F red), but evoked PSC amplitude is not reduced as compared to control (control: Figs. 6A, C; ΔI-IIA: Figs. 6E, G). Normal PSC amplitudes at reduced mPSC amplitudes are caused by a compensatory increase in mean quantal content (control: Fig. 6D; *ΔI-IIA*: Fig. 6H). By contrast, PHP is not observed upon removal of the *I-IIB* exon (Figs. 6I-L). As in controls and in *ΔI-IIA* animals, PhTx application reduces mPSC amplitude by ~0.2 nA as expected (Figs. 6B, F, J), but in *ΔI-IIB* no compensatory increase in mean quantal content is observed (Fig. 6L), so that PSC amplitude is not restored to its original setpoint (Fig. 6K). Similarly, in *ΔI-IIB* animals, PHP is also not possible in response to a permanent reduction of glutamate receptor function in *GluRIIA* mutants, which has been named PHP maintenance and is genetically separable from PHP induction (James et al. 2019). In *GluRIIA* mutants, compensatory upregulation of mean quantal content is observed in animals with GFP-tagged Ca_v2 and upon excision of *I-IIA*, but not following excision of the *I-IIB* exon (Fig. 6M). Therefore, the lack of the *I-IIB* exon causes fewer Ca_v2 calcium channels in the AZ and impairs both PHP initiation and maintenance.

Given that synapses that contain only Ca_v2 isoforms without the *I-IIB* exon show a lower release probability, more variable paired pulse ratios and synaptic depression, and an inability for compensatory increases in mean quantal content, the question arises whether normal synapses contain the I-IIA containing Ca_v2 channels at all. This can be tested in transheterozygous $\Delta I\text{-}IIA^{GFP}/\Delta I\text{-}IIB^{mEOS4b}$ animals, which show normal PSC amplitudes as well as mPSC amplitudes and frequencies (Figs. 3J-L). Co-labeling of active zones with anti-brp (Fig. 6N, cyan) in animals that contain Ca_v2 channels without I-IIB but with GFP-tagged I-IIA (Fig. 6N, green) on one chromosome and Ca_v2 channels without I-IIA but with mEOS4b-tagged I-IIB (Fig. 6N, magenta) indicates that all active zones contain Ca_v2 with I-IIB, most contain both I-IIB and I-IIA, but few active zones contain Ca_v2 channels with only I-IIA (Fig.

6N, white arrowheads). Quantification reveals that ~95 % of all active zones contain Ca_v2 channels with both, the I-IIA and the I-IIB exon, less than 5 % of the active zones contain only Ca_v2 with the I-IIB exon and no active zone contains only Ca_v2 with the I-IIA exon. These data show that the vast majority of presynaptic active zones house a mixture of I-IIA and I-IIB Ca_v2.

Discussion

The Drosophila *Ca_v2* homolog is named *cacophony* and contains two mutually exclusive splice sites that do not exist in vertebrate *Ca_v2* VGCC genes. Our data show that alternative splicing at these sites substantially increases Drosophila Ca_v2 functional heterogeneity. We report that the first mutually exclusive exon, that is located in the fourth transmembrane domain of the first homologous repeat (*IS4*), affects Ca_v2 biophysical properties and is decisive as to whether the channels localize to presynaptic active zones (AZs) and thus participate in fast synaptic transmission. By contrast, mutually exclusive splicing at the second site encoding the intracellular linker between the first and the second homologous repeat (I-II) does not affect Ca_v2 presynaptic active zone localization, but instead, fine-tunes multiple different aspects of presynaptic function. In vertebrates, substantial functional synaptic heterogeneity can result from different combinations of $Ca_v2.1$, $Ca_v2.2$, and/or $Ca_v2.3$ in the presynaptic AZ (reviewed in Zhang et al. 2022). In Drosophila, the collective functions of mammalian $Ca_v2.1$, $Ca_v2.2$, and $Ca_v2.3$ must be portrayed by one *Ca_v2* gene. Mutually exclusive splicing at the *IS4* and *I-II* sites might have been a different evolutionary strategy to create Ca_v2 mediated functional synaptic heterogeneity. Below, we will discuss the consequences of Drosophila *Ca_v2* splicing at these sites for presynaptic function.

Exon IS4B is required for sustained HVA current and presynaptic AZ localization

Mutually exclusive splicing in the 4th transmembrane domain of the first homologous repeat (*IS4*) yields either *IS4A* or *IS4B*. Our data show that the *IS4B* exon is required for presynaptic AZ localization of Ca_v2 and for evoked synaptic transmission at a fast glutamatergic synapse, the Drosophila NMJ. Accordingly, excision of the *IS4B* exon is embryonic lethal. This is in accordance with the finding that the only Ca_v2 knock-in construct that has ever been reported to rescue lethality of Drosophila *Ca_v2* null mutants contains the *IS4B* exon (*UAS-cac1*; Kawasaki et al. 2004). The other alternative exon at the *IS4* site, *IS4A*, is not sufficient to mediate presynaptic AZ localization, does not contribute to evoked synaptic transmission at fast synapses, but it gives rise to functional Ca_v2 that localize to other neuron types and neuronal compartments. Accordingly, animals with excision of *IS4A* show largely normal neuromuscular transmission but impaired motor behavior and reduced vitality in the adult (not shown).

Our voltage clamp recordings from motoneuron somata show that splicing in the 4th transmembrane domain, where the voltage sensor is located, affects Ca_v2 activation voltage. Removing the *IS4B* exon virtually abolishes fast activating, sustained Ca_v2 mediated HVA current. We infer that IS4B containing Ca_v2 mediate fast activating, sustained HVA current also in presynaptic active zones, although we cannot exclude the possibility that IS4B Ca_v2 interacts with different accessory calcium channel subunits or with different other proteins to give rise to macroscopically different calcium currents, depending on whether the Ca_v2 α_1-subunit localizes to presynaptic AZs, or to other subcellular compartments. However, fast activating, sustained HVA current is in accordance with the demands of the Drosophila larval NMJ that transmits burst of ~200 ms duration with action potential frequencies of ~120 Hz during crawling (Kadas et al. 2017). Fast voltage gated activation of sustained HVA calcium current with fast inactivation upon repolarization is useful at large intraburst firing frequencies without excessive Ca_v2 inactivation. Our somatic voltage clamp recordings further demonstrate that IS4B is not only essential for evoked synaptic transmission, but Ca_v2 with the IS4B exon can also give rise to somatodendritic HVA current. Therefore, the *IS4B* exon is essential for presynaptic function but it can

also give rise to Ca_v2 currents in other neuronal compartments. By contrast, the *IS4A* exon is used exclusively outside the presynaptic AZ of fast synapses for yet uncharacterized Ca_v2 functions.

I-II exon alternative splicing fine-tunes presynaptic function

In contrast to the *IS4* exon, mutually exclusive splicing in the intracellular loop between the first and the second homologous repeat (I-II) does not affect Ca_v2 localization in AZs at the NMJ. In fact, >95 % of all presynaptic AZs contain both, Ca_v2 isoforms with I-IIA and Ca_v2 isoforms with I-IIB. Single on-locus alternative exon removal at the *I-II* site allows the study of presynaptic Ca_v2 channel function with only one of the mutually exclusive I-II exons. Removal of *I-IIA* (*ΔI-IIA*) leaves 8 isoforms that contain *I-IIB*. This does not affect Ca_v2 localization or channel number in presynaptic AZs as compared to control. However, half amplitude width of evoked PSCs is significantly decreased whereas median amplitude of evoked PSCs is increased from ~115 nA to ~130 nA, although the amplitude increase is statistically just not significant (one sided Mann Whitney U-test, $p = 0.078$). Similar channel numbers and localizations but altered PSC amplitudes and shapes indicate different Ca_v2 properties in the absence of *I-IIA* as compared to control. Specifically, decreased PSC half width could be caused by significantly faster channel inactivation kinetics, and slightly increased single channel conductance may increase PSC amplitude. Alternatively, altered PSC width and amplitude could also be caused by changes in presynaptic action potential shape or postsynaptic glutamate receptor properties or compositions. However, given that *I-IIA* excision primarily affects the relative abundance of I-IIA and I-IIB Ca_v2 in the presynaptic AZ but not mean channel number, because postsynaptic VGCCs in muscle are encoded by the Drosophila *Ca_v1* and *Ca_v3* homologs, and Ca_v2 localize to axon terminal AZs, we judge different properties of different Ca_v2 isoforms the most parsimonious explanation for altered PSC properties upon *I-IIA* excision. During repetitive firing, the median increase of PSC amplitude by ~10 % is likely counteracted by the significant decrease in PSC half amplitude width by ~25 %, so that neither paired pulse ratios, nor synaptic depression show significant differences between control and *ΔI-IIA*. Even for stimulus trains that mimic intraburst motoneuron activity as observed during restrained crawling in semi-intact preparations (Kadas et al. 2017), there is no difference in charge transfer from the motoneuron axon terminal to the postsynaptic muscle cell between *ΔI-IIA* and control. Surprisingly, crawling is significantly affected by the removal of *I-IIA*, in that the animals show a significantly increased mean crawling speed but no significant change in the number of stops. Given that the presynaptic function at the NMJ is not strongly altered upon *I-IIA* excision, and that *I-IIA* likely mediates also Ca_v2 functions outside presynaptic AZs (see above) and in other neuron types than motoneurons, and that the muscle calcium current is mediated by *Ca_v1* and *Ca_v3*, the effects of *I-IIA* excision of increasing crawling speed is unlikely caused by altered pre- or postsynaptic function at the NMJ. We judge it more likely that excision of *I-IIA* has multiple effects on sensory and pre-motor processing, but identification of these functions is beyond the scope of this study.

Removal of *I-IIB* (*ΔI-IIB*) leaves 10 Ca_v2 isoforms that contain I-IIA. This does not affect presynaptic AZ localization of Ca_v2 or the proximity to the AZ scaffold protein brp (Kittel et al. 2006), but it significantly reduces P_r by ~ 50 %. This bisection in P_r is correlated with a 50 % reduction in the number of Ca_v2 in AZs from about 10 to about 5, as determined by tagged Ca_v2 fluorescence intensity measurement in fixed specimen and by live sptPALM counting of Ca_v2^{mEOS4b} (Heck et al. 2019; Ghelani et al. 2023). These data suggest that P_r is nearly linearly related to the number of VGCCs in the presynaptic AZ. This has recently also been suggested within NMJ synapse-type, based on correlative measurements of P_r and

tagged Ca_v2 fluorescence intensity measurement (Medeiros et al. 2023, bioRxiv). This also corresponds to observations at the mammalian calyx of Held, where the number of AZ VGCCs correlates linearly with P_r, and moreover, influences whether subsequent release is depressed or facilitated (Sheng et al. 2012). Similarly, in synapses with fewer Ca_v2 channels upon *I-IIB* excision, we find a significant decrease in P_r along with a significant reduction in paired pulse depression. Therefore, regulation of VGCC number in presynaptic AZs may be a conserved mechanism to tune P_r and short-term plasticity from flies to mammals.

At the Drosophila NMJ a steep gradient of synaptic transmission amplitude exists along the motoneuron axons over their target muscle fibers, with the highest presynaptic Ca^{2+} influx in most distal presynaptic sites along the axon. This has been interpreted as gradient control of P_r along the axon of the same neuron (Guerrero et al. 2005), which is at least in part regulated by the balance of different release enhancing and suppressing proteins at proximal versus distal release sites, such as complexin (Newman et al. 2022). Another potential means to regulate P_r at different release sites of the same neuron could be uneven ratios of I-IIA and I-IIB Ca_v2 isoforms, which requires additional analysis. The prediction would be that the more distal the release site the more I-IIB channels are expressed. Given that these have a highly conserved Ca_β binding motif, targeting to distal release sites might be promoted in comparison to I-IIA channels with a less conserved Ca_β binding motif (Smith et al. 1998).

The reduction in AZ Ca_v2 number upon removal of *I-IIB* has three additional important functional consequences. First, reduced P_r and charge transfer across the NMJ during crawling-like motoneuron bursting patterns are reflected in a significant decrease in mean crawling speed and a highly significant increase in the number of stops, whereas maximum crawling speed is not affected. Unaffected maximum speed at significantly reduced P_r indicates that the charge transfer at high motoneuron intrabust firing frequencies is above the one needed for maximum muscle contraction. Moreover, mean speed is significantly but just slightly decreased upon removal of *I-IIB* and a highly significant reduction in P_r, whereas the number of stops is increased highly significantly by ~50 %. It seems likely that large effects on the continuation of motor behavior but only mild effects on the speed are caused not only by effects on synaptic transmission at the NMJ but also by effects on other neuronal compartments or on other neurons in sensory or premotor circuitry. This interpretation would be in accordance with the finding that Ca_v2 currents are also measured from the somatodendritic domain of pupal and adult Drosophila (this study) and that larval Drosophila motoneuron excitability as measured by I/F relationships are altered upon *Ca_v2*-RNAi (Worrell, Levine, 2008). Second, removal of *I-IIB* increases the variability of paired pulse ratio and the time course of synaptic depression. It seems plausible that mechanism with probabilistic features, such as Ca_v2 activation/inactivation/de-inactivation as well as Ca_v2 channel mobility in AZs (Heck et al. 2019; Ghelani et al. 2023) exert a higher impact with fewer channels. Therefore, increasing variability of presynaptic function might be another consequence of reduced AZ Ca_v2 number upon *I-IIB* excision. And third, removal of *I-IIB* abolished the ability of both initiation and maintenance of presynaptic homeostatic potentiation (PHP), which in turn, requires an upregulation of the number of Ca_v2 and of brp molecules in the presynaptic active zone (Ghelani et al. 2023). Increasing the number of I-IIA Ca_v2 in AZs as a compensatory response to reduced postsynaptic receptor function seems not likely with reduced Ca_β binding affinity, or in the face of fewer channels to start with, or for additional reasons, which will require additional studies.

In summary, our study suggests mutually exclusive splicing at two *Ca_v2* splice sites, that do not exist in mammals, as an alternative strategy to increase functional heterogeneity at the presynaptic AZ of fast chemical synapses, so that the Drosophila *Ca_v2* homolog *cacophony* may portrait some of the

functional heterogeneity that arises in mammals from the combinatorial usage of $Ca_v2.1$, $Ca_v2.2$, and $Ca_v2.3$. Splicing at the first Drosophila mutually exclusive site directs Ca_v2 to different subcellular compartments and tunes IS4B Ca_v2 biophysical properties. Splicing at the second mutually exclusive site does not direct Ca_v2 to different subcellular compartments, but it fine tunes multiple aspects of presynaptic function by changing presynaptic AZ channel numbers or ratios between Ca_v2 splice variants.

Methods

Generation of CRISPR flies:

Exon excision was performed via the CRISPR/Cas9 method (Doudna and Charpentier, 2014; Sternberg and Doudna, 2015). Ca_v2 in Drosophila is located on the X-chromosome. Ca_v2^{sfGFP} exon out flies were generated by crossing female virgin flies expressing super folder GFP (sfGFP)-tagged Ca_v2 (Ca_v2^{sfGFP}, Gratz et al. 2019) channels along with the Cas9 enzyme under the control of the germ line active *nanos*-promoter (*nos-cas9*, Bloomington stock center #78781) to male flies expressing a *gRNA* transgene under the control of the germ line active *U6*-promoter. The *gRNA* sequences were designed such to specifically target sequences flanking the exon to be excised (see table 1). CRISPR events take place as soon as both *nos-cas9* as well as *U6-gRNA* transgenes are present in the same fly, no matter whether these flies are male or female. For simplicity, for excision of exons *IS4A*, *I-IIA*, and *I-IIB*, male progeny were collected as such flies are hemizygous vital, whereas for excision of *IS4B*, females were collected because removal of *IS4B* is lethal. Flies were then back-crossed into suitable balancer strains to keep the X-chromosome with the putative Ca_v2 exon excision and to be able to follow out-crossing of *nos-cas9* or *U6-gRNA* transgenes. Successful exon excision was confirmed with single fly genomic PCR with suitable primers and Taq DNA polymerase (New England Biolabs, #M0267S) (for cycler (Biorad T100 thermo cycler) settings and primers see tables 2 and 3) and subsequent 1% agarose gel electrophoresis. Gene sequence around the excision was confirmed with next generation sequencing (StarSeq, University of Mainz Campus with the exon out verification primers, see table 3). Gels were run at 100 V for 45 minutes. Primers were obtained from Integrated DNA Technologies, Germany. To minimize contamination of exon out fly stocks, successful excision mutants were cantonized for at least 5 generations to enhance the likelihood of outcrossing of undesired mutations due to CRISPR off-target events. To clean up the X-chromosome itself on which the desired CRISPR event took place, flies were subjected to recombination with CantonS flies. Lack of the desired exon was then re-confirmed by PCR again.

Table 1: gRNA sequences used for cas9 target site. Vertical lines depict intended break points. Bold and underlined nucleotides indicated PAM (protospacer adjacent motif) sequences.

target exon	pre-exon	post exon
IS4A	**cca**atatcacctatg|tttaagtc	gttgctac|taccaaaaacct**agg**
IS4B	**ccg**aaactatagagt|gactgacc	gtggcaca|tgattgtcgtgg**agg**
I-IIA	gctacgtg|catgtgcataca**cgg**	**cca**agtaaactgcca|taatcaac
I-IIB	**cca**gtaaatgatttc|gactttct	**ccc**ccatatgttcat|ccacatcc

Table 2: Cycler settings for exon out verification.

Step	temperature		duration
1	95°C		3:00 min
2	95°C		0:30 min
3	57°C	-1°C per cycle	0:45 min
4	68°C		1:30 min
5	Go to step 2	10x	
6	95°C		0:30 min
7	52°C		0:45 min

8	68°C		1:30 min
9	Go to step 6	24x	
10	68°C		5:00 min
11	4°C		∞

Table 3: Exon out verification primers

excised exon	forward primer	reverse primer	expected band size with/without exon
IS4A	CACGCCGTGCAAGCATTATC	CCTAAATTCGTGGCTACCAC	988 bp/482 bp
IS4B	CTGTGTGTGATTCTCGCGAC	CCGTTCCGATTCGATCCAG	1305 bp/340 bp
I-IIA	GCCACTTCTACACCAGTTCAC	GAACTCTTTGTAGCCGGG	951 bp/571 bp
I-IIB	CTCATTGAAGGTTCCCGTC	GGAGAGGGATGCTAAGAATG	954 bp/446 bp

Generation of gRNA transgenic flies:

First, the eligibility for Cas9 cleavage was assessed, core properties are the protospacer adjacent motif (PAM) NGG flanking the 20 bp *gRNA* (see table 1) to facilitate site recognition, and a 5' G as the vector used for *gRNA* expression later used the *U6*-promoter. Moreover, CRISPR sites must not disrupt recognition sites for the splicing machinery. For this, online tools were used (CRISPR target finder: Gratz et al. 2014, http://targetfinder.flycrispr.neuro.brown.edu/index.php and Cas9 target finder: https://shigen.nig.ac.jp/fly/nigfly/cas9/cas9TargetFinder.jsp). Sites for double strand breaks were picked at a distance from the intron/exon borders to not affect splice acceptor sites. Furthermore, sites known to impact splice efficiency (Blanchette et al. 2005; Brooks et al. 2011) were avoided. In addition, sites for minimal loss of total genomic region were determined and the *gRNA* sequences with as few as possible predicted off-target cleavage sites were selected.

Fly rearing

Flies were kept at 25°C in 25 mm diameter plastic vials with mite proof foam stoppers on a cornmeal, yeast, agar, glucose diet on a 12 hr light/dark regimen. Wandering L3 larvae were collected directly from food vials. 2-day old adult flies were collected from their food vials and placed on ice in pre-chilled empty food vials for no more than 1 minute prior to dissection (for patch clamp recordings).

Flies

For electrophysiological recordings as well as for immunohistochemical labeling, sfGFP-tagged Ca_v2 flies were used. First, validity of sfGFP-tagged Ca_v2 channel flies was confirmed by comparing w^+ TI{TI}$cac^{sfGFP\text{-}N}$ flies with the wildtype strain Canton special (Canton S). After that, the control strain for all sfGFP-tagged exon out flies was w^+ TI{TI}$cac^{sfGFP\text{-}N}$

Exon out flies were w^+ TI{TI}$cac^{sfGFP\text{-}N\ \Delta IS4A}$, w^+ TI{TI}$cac^{sfGFP\text{-}N\ \Delta IS4B}$/FM7c P{2x Tb-RFP}, w^+ TI{TI}$cac^{sfGFP\text{-}N\ \Delta I\text{-}IIA}$, w^+ TI{TI}$cac^{sfGFP\text{-}N\ \Delta I\text{-}IIB}$. All CRISPR fly strains were originally white mutant. To reduce the likelihood of accumulation of off-target effects resulting from CRISPR events, we replaced the mutant white gene on

the X-chromosome (on which cacophony is also located) by a Canton S derived wildtype white gene from our Canton S lab stock that we also used as control (see above). In addition, after CRISPR events, flies were crossed to remove nos-Cas9 and gRNA transgenes on the 2nd chromosome and replaced these chromosomes by ones without transgenes or other known mutations. This first removed transgenes that were needed for CRISPR induction and second, this also removed possible off target events on the 2nd chromosome. In the process, 3rd and 4th chromosomes were replaced automatically as well. We back crossed with CantonS strains for at least 5 generations. Thus, off-target chromosomal aberrations were minimized by recombination on the X-chromosome and by replacement of all other chromosomes by out-crossing.

For channel counting and for assessment of $Ca_v2^{I\text{-}IIA}$ and $Ca_v2^{I\text{-}IIB}$ expression in active zones (both see below), we used exon out flies that carried mEOS4b endogenously directly after the start codon of fly Ca_v2 *cacophony* (Ghelani et al. 2023). mEOS4b-tagged exon out fly strains were: w* TI{TI}cac$^{mEOS4b\text{-}N}$, w* TI{TI}cac$^{mEOS4b\text{-}N\ \Delta I/IIA}$, w* TI{TI}cac$^{mEOS4b\text{-}N\ \Delta I/IIB}$. All mEOS4b-tagged fly strains were white mutant.

Western Blots

For proof of protein expression after exon excision, Western Blots were performed with detection of the N-terminal sfGFP tag (due to lack of cacophony antibodies). As loading control, β-actin was used. Cacophony bands were expected above 250 kDa (cacophony plus GFP) and actin was expected at 42 kDa. For viable exon excision mutants (cac^{sfGFP} as control, cac$^{sfGFP\ \Delta IS4A}$, cac$^{sfGFP\ \Delta I\text{-}IIA}$, cac$^{sfGFP\ \Delta I\text{-}IIB}$), 10 adult male brains per lane were prepared, for lethal exon excisions (Canton S as control, cac^{sfGFP}/+, cac$^{sfGFP\ \Delta IS4B}$/+), 20 adult female brains of heterozygous animals were used. Brains were dissected with forceps one by one and collected in 23 µl squishing buffer (composition below) in 0.5 ml low bind sample tubes on ice. When 10 or 20 brains, respectively, were collected, samples were squished with a sterile pestle using a motorized squishing device. After squishing, 3 µl sample buffer (composition below) were added to the homogenized samples, which were subsequently boiled at 95°C for 5 min. Samples were then stored at -30°C until use. For loading, samples were taken out of the freezer, boiled for 3 minutes at 95°C and directly loaded into a 10 well Mini-Protean TGX Precast Gel with a 4-15% polyacrylamide gel gradient with 50 µl volume per well (Biorad, Cat#456-1084). The gel was run in running buffer (composition below) for 2h 40 minutes at 80 V. As protein marker, 8 µl Spectra Multicolor High Range Ladder (Thermo Scientific, Cat# 26625) was used. Transfer was done in transfer buffer (composition below) on nitrocellulose membrane overnight at 35 V with a cool block and the setup sitting in an ice box. Next day, the nitrocellulose membrane was washed with TBS-Tween20 and then subjected to blocking with Intercept T20 Antibody Diluent (LI-COR, Cat#927-65001) diluted 1:1 with 0.1M PBS for 2 hrs. Then the nitrocellulose membrane was cut horizontally to subject the pieces with the expected cacophony bands and the expected loading control (β-actin) separately to antibody labeling. This was followed by primary antibody incubation with 1:500 polyclonal rabbit anti-GFP antibody (Thermo Fisher Scientific, Cat# A11122) or 1:10,000 monoclonal mouse anti-actin (DSHB, JLA20) diluted in Intercept T20 Antibody Diluent (see above), first for 2 hrs at room temperature and then for two nights at 4°C. Then antibody solution was removed and membrane washed 3x 15 minutes with TBS-Tween20. This was followed by incubation with secondary antibodies diluted in Intercept T20 Antibody Diluent for 2 hrs at room temperature in the dark with IRDye 680 donkey anti-rabbit (LI-COR, Cat# 926-68073) at 1:10,000 to detect GFP-tagged cacophony bands, or IRDye 800 donkey anti-mouse 1:10,000 to detect β-actin, respectively. This was followed by 2x 15 minutes washes with TBS-Tween20 and then 1x 15

minutes with 0.1M PBS to reduce background. Bands were detected with a LI-COR Odyssey Fc Imaging System with 30 second or 2 minutes exposure times.

Western Blot solutions:

Lyse buffer: 25 ml 4xTris-HCl/SDS pH 6.8, 20 ml glycerol, 4 g SDS, 1 mg bromophenol blue.

6x sample buffer (10 ml): 0.3 M Tris-HCl pH 6.8, 8% SDS, 50% glycerol, 0.25% bromophenol blue. 8% mercapto-ethanol was added fresh directly before use.

10x SDS running buffer: 30 g Tris Base (pH 8.3), 150 g glycine, 10 g SDS. Add ddH_2O to 1000 ml total volume.

Transfer buffer: 15.5 g Tris Base, 72 g glycine, 1000 ml methanol, 5000 ml ddH_2O.

Dissection for electrophysiology and immunohistochemical labeling

Third instar larvae were dissected in HL3.1 saline (composition below). Larvae were fixed dorsal side up to a Sylgard (Sylgard 184, DowCorning) coated lid of a 35 mm Falcon dish with two insect minuten pins through the mouth hook and through the tail. After covering the larva with saline (composition below), the body wall was cut along the dorsal midline. To obtain a filet preparation, the body wall was spread laterally and fixed with two minuten pins on each side. Gut and trachea were removed as well as the ventral nerve cord. For electrophysiology from the larval NMJ (see below: electrophysiology), the motor nerves were left long, for immunohistochemical labeling (see below: immunohistochemistry), the motor nerves were cut very short.

Adult flies were dissected in normal saline (composition below – but calcium current recordings were performed with different external solution – composition and electrophysiology see below). Adult two-day old female flies were anaesthetized briefly on ice in pre-chilled empty fly rearing vials. Then legs and wings were removed and the fly fixed dorsal side up in a Sylgard coated lid of a 35 mm Falcon dish with two insect minute pins through the head and through the tip of the abdomen. After covering the fly with saline (composition below), the cuticle was cut along the dorsal midline. To expose the ventral nerve cord with the motoneurons, the thoracic cuticle with the cut wing depressor muscle (DLM) was spread laterally and pinned down with one minuten pin on either side. After removal of gut, esophagus, and salivary glands, the ventral nerve cord was exposed.

Electrophysiology

All electrophysiological recordings were carried out at room temperature (~ 22°C). For TEVC recording microelectrodes were pulled with a Sutter Flaming Brown P97 microelectrode puller from borosilicate glass capillaries with filament, with inner diameter of 0.5 mm, and an outer diameter of 1 mm (Sutter BF100-50-10 or World Precision Instruments 1B100F-4). Patch pipettes were pulled with a Narishige PC10 electrode puller from borosilicate glass capillaries without filament, with an inner diameter of 1 mm, and an outer diameter of 1.5 mm (World Precision Instruments PG52151-4).

TEVC of muscle 6 or muscle 12 in the larval body wall

For two electrode voltage clamp (TEVC) recordings, dissected third instar larvae (see dissection) were placed on an upright Olympus BX51WI fixed stage microscope with a 20x water dipping lens (Zeiss LD A-Plan). The motor nerves of either segment A2 or A3 on the left or the right side was sucked into a glass microelectrode filled with saline with an individually broken tip. After placing the recording electrodes filled with 3 M potassium chloride (KCl) and the ground wire (chlorinated silver) into the recording solution (HL3.1 saline, composition see below), both electrodes were nulled against the ground electrode (bridge mode) using an Axoclamp 2B intracellular amplifier (Molecular Devices). Then the muscle (M6 or M12) cell was first impaled with the larger tip current passing glass microelectrode (~8 - 13 MΩ) directly followed at a small distance by the smaller tip recording electrode (~20 - 30 MΩ). If both electrodes recorded a membrane potential of at least -50 mV without differing by more than 3 mV, RMP balance was adjusted and then TEVC established by pressing the respective knob on the amplifier. Gain was set between 8 and 25. Anti-alias filter was set to ½ the sampling rate to minimize noise. Then the desired command potential was set, mostly at -70 mV. Holding current needed to keep the membrane potential at the desired -70 mV had to be below 4 nA, otherwise recordings were discarded. Data were digitized at 50 kHz (Digidata 1550B, Molecular Devices) and recorded with pClamp 11.1.0.23 software package (Molecular Devices). Data were filtered offline with a lowpass Gaussian Filter with a -3 dB cutoff frequency of 360 Hz.

The suction electrode with the motor nerve was connected to a pulse generator (A-M Systems Model 2100) to deliver low voltage (up to 10 V) 0.1 ms duration stimulations at varying patterns. Stimulation voltage was adjusted slowly to be sure that both motor axons innervating the recorded muscles were stimulated. This was determined unequivocally by the transmission amplitude, which is distinctly smaller if just one motor axon is stimulated as compared to stimulation of both motor axons.

For recordings of miniature excitatory postsynaptic currents (mEPSCs), spontaneous occurrence of mEPSCs was recorded for one minute without stimulation. For single evoked excitatory postsynaptic currents (EPSCs), the motor nerve was stimulated at 0.1 Hz frequency for 50 seconds and the amplitude was recorded. Mean quantal content was determined by dividing the mean amplitude of several EPSCs of one recording by the mean amplitude of several mEPSC of the same recording. For short term plasticity, paired pulses (PPs) were recorded by stimulation of the motor nerve twice with varying interspike intervals (IPIs) of 10 ms, 15 ms, 20 ms, 25 ms, 30 ms, 50 ms, and 100 ms. Short term facilitation or short term depression were induced by 60 s stimulation at 1 Hz or by 1s stimulation at 5 Hz, 10 Hz, 20 Hz, 40 Hz or by 200 ms stimulation at 60 Hz and 120 Hz stimulation frequency. Motoneuron burst firing as occurring during crawling (Kadas et al. 2017) was simulated by higher frequency stimulation for 200 ms at 60 Hz and 120 Hz.

Presynaptic homeostatic potentiation (PHP) was induced either acutely by application of the bee wolf toxin Philanthotoxin 433 or by using animals carrying a null mutation in the GluRIIA glutamate receptor that is expressed in the muscle membrane. PhTx (10 µM) is applied in calcium-free HL3.1 saline (composition see below) after dissection but before mounting the preparation on the microscope stage. For the toxin to work properly, it must be applied after cutting the animal open along its dorsal midline but prior to spreading the larval body wall laterally (see dissection). The larva must be fixed with two minuten pins through the mouth hooks and the tail but without stretching the animal and without removing any inner organs yet. The preparation is bathed in the toxin solution for 10 minutes. After rinsing the preparation with HL3.1 saline, the body wall is spread laterally and dissected as

described above (see dissection), and the specimen is mounted on the microscope stage ready for recording.

Synaptic transmission on muscle M6 in segment A2 and A3 was assessed in male animals carrying excisions of either IS4A, I-IIA, or I-IIB in Ca_v2 on their only X-chromosome. Animals lacking exon IS4B are homozygous lethal. Thus, we used heterozygous females that expressed Ca_v2 with IS4B excision on one X-chromosome over a Ca_v2 FLPStop construct which contains a tdTomato reporter followed by a stop codon within the open reading frame of all Ca_v2 variants upon expression of a flipase transgene. Briefly, a reverse stop cassette followed by UAS-tdTomato flanked by canonical FRT sites of opposing orientation is inserted within a MiMIC residing in an intron of the Drosophila Ca_v2 channel gene *cacophony*. Presence of canonical flipase turns the entire FlpStop-tdTomato cassette around and-re-inserts it in frame, which leads to pre-mature termination of Ca_v2 transcription that is reported by tdTomato (Fisher et al. 2017). We expressed UAS-flipase under the control of the OK6 (Rapgap1)-GAL4 driver (Sanyal 2009), that drives expression of UAS-transgenes also in larval crawling motoneurons.

However, in our hands, flp events happen in a more or less stochastic manner. Flp events in motoneurons on M6 are less reliable as compared to Flp events on M12. As it is necessary that the FlpStop technique works in all motoneurons that innervate a target muscle to investigate the role of the IS4B exon for synaptic transmission, we used M12 (left and right) in A3 for this experiment rather than M6.

Whole cell voltage clamp recordings

To investigate calcium currents that remain upon excision of IS4B, we used the same FlpStop approach as for synaptic transmission at the larval NMJ. UAS-flipase was expressed under the control of a DLM (dorsal longitudinal muscle) motoneuron Split-GAL4 fly strain that targets mainly the 5 wing depressor motoneurons (MN1-5) on each side of the body (10 neurons total, Hürkey et al. 2023). Expression of UAS-flipase under the control of this Split-GAL4 driver reliably led to expression of tdTomato in these motoneurons. In addition these flies are fligh-less.

Adult MN patch clamp experiment were carried out as previously reported (Ryglewski et al. 2012). After dissection, the fly was positioned under a 40x water dipping lens (Zeiss, W Apochromat 40x/1.0 DIC VIS-IR ∞/0) on a fixed stage Zeiss AxioExaminer A1 upright fluorescence microscope. MN5 is situated on the dorsal surface of the ventral nerve cord in the mesothoracic neuromere. For whole cell voltage clamp recordings from MN5, protease was applied focally by alternating positive and negative pressure applied through a broken patch pipette to clean the membrane of the MN5 soma to facilitate seal formation. After cleaning, the preparation was perfused constantly with fresh saline (composition below). Voltage gated potassium channels were blocked by TEA, 4-AP and cesium in the recording solution (composition below). Tetrodotoxin (TTX, 10^{-7} M) to block voltage gated sodium channels was applied directly to the recording chamber while perfusion was halted for 3 minutes before approaching the cell with the patch pipette. Then perfusion resumed. Patch pipettes were filled with internal patch solution (composition below) and had resistances of ~ 3.5 – 4 MΩ with this combination of internal and external solution. Recordings were carried out with an Axopatch 200B patch clamp amplifier (Molecular Devices). Data were digitized at 50 kHz (Digidata 1440, Molecular Devices) and filtered at 5 kHz through a lowpass Bessel filter. Data were recorded with pClamp 10.7.0.3 software package (Molecular Devices). After giga seal formation, whole cell configuration was achieved by a brief application of

negative pressure to the patch pipette. We allowed 2 minutes for solution exchange with the cell interior and stabilization of the recording before adjusting whole cell capacitance and series resistance compensations and setting prediction at around 80% and correction at around 45%. Holding potential was -70 mV between voltage clamp protocols. Voltage gated calcium currents were elicited by voltage command steps to +20 mV in 10 mV increments from a holding potential of -90 mV. Leak was subtracted offline.

Dissection and electrophysiology salines:

Adult dissection saline [mM]: NaCl 128, KCl 2, $CaCl_2$ 1.8, $MgCl_2$ 4, HEPES 5, Sucrose ~35.5. Osmolality was adjusted to 300 mOsM/kg with sucrose. pH was adjusted to 7.24 with 1N NaOH.

Larval dissection saline HL3.1 calcium free [mM]: NaCl 70, KCl 5, $MgCl_2$ 4, $NaHCO_3$ 10, trehalose 5, sucrose 115, HEPES 5. Osmolality was adjusted to 300 mOsM/kg with sucrose. pH was adjusted to 7.24 with 1N NaOH.

TEVC recording saline HL3.1 [mM]: NaCl 70, KCl 5, $CaCl_2$ 0.5, $MgCl_2$ 4, $NaHCO_3$ 10, trehalose 5, sucrose 115, HEPES 5. Osmolality was adjusted to 300 mOsM/kg with sucrose. pH was adjusted to 7.24 with 1N NaOH.

Whole cell voltage clamp saline [mM]: NaCl 93.2, KCl 5, $MgCl_2$ 4, $CaCl_2$ 1.8, $BaCl_2$ 1.8, Tetraethylammonium (TEA) Cl 30, 4-aminopyridine (4-AP) 2, HEPES 5, sucrose ~35.5. Osmolality was adjusted to 300 mOsM/kg with sucrose. pH was adjusted to 7.24 with 1N NaOH.

Tetrodotoxin (10^{-7}M) in normal saline was applied directly to the recording chamber.

Whole cell voltage clamp intracellular solution [mM]: CsCl 144, $CaCl_2$ 0.5, EGTA 5, HEPES 10, TEA-Br 20, 4-AP 0.5, Mg-ATP 2. Osmolality was adjusted to 300 mOsm/kg with glucose. pH was adjusted to 7.24 with 1N CsOH.

mEOS4b-tagged Ca_v2 channel counting

The calculation of Ca_v2 channel splice form numbers in individual active zones of the NMJ are based on the photoconversion of the fluorescent tag mEOS4b fused to the N-terminus of the Ca_v2 channel (Ca_v2::mEOS4b-N; Ghelani et al. 2023). Third instar larvae were used for a body wall dissection (Marter et al. 2019). This preparation was suitable to image individual active zones within single boutons of an NMJ. We focused on muscle 6/7 on large type Ib boutons (Jia et al. 1993). Experiments were conducted at 25°C with HL3.1 solution (composition see above). We used a TIRF setup based on an inverted microscope (Nikon Eclipse Ti) equipped with a 60x 1.49 NA oil immersion objective (Nikon). Image series of up to 5000 frames were acquired at a frame rate of 20 Hz, using a sCMOS camera (Hamamatsu, Orca flash 4.0) controlled by the NIS-Element acquisition software (Nikon). Labelling of the NMJ with an anti-HRP antibody (diluted 1:1000) directly tagged with Alexa-488 for 5 min was used to have an initial landmark for NMJs within the preparation. During imaging of Ca_v2 channels, we use a 1.5 magnification lens to reduce the effective pixel size to 71 x 71 nm. The used illumination protocol started with an initial continuous illumination with a 561 nm laser (80 % of initial laser power of 100 mW) for 250 frames to reduce the autofluorescent background. Afterward, we triggered the photoconversion of mEOS4b by switching on the photoconversion with a 405 nm UV-laser (5% of initial

laser power of 100 mW) in addition to the 561 nm laser. The UV-excitation was sufficient to convert the majority of mEOS4b molecules into the red fluorescent state that was read out by the 561 nm laser. With the dual excitation of 405 nm and 561 nm, synapses were imaged until complete bleaching of the Ca_v2::mEOS4b-N population. The ability of the TIRF setup to adjust the laser beam orientation in the specimen was used to obtain an oblique illumination profile that limited the contribution of out of focus fluorescence. The number of channels was calculated as ratio of the maximal fluorescent intensity shortly after starting the photoconversion and the fluorescence of single mEOS4b molecules, which occurred as stochastic blinking events in the second half of the illumination sequence (see Fig. 4G, Ghelani et al. 2023). Two-dimensional x-y movements of the NMJ was corrected by using the NanoJ-Core drift correction from the NanoJ-Plugin for ImageJ/Fiji (Laine et al. 2019). After background subtraction, regions of 5x5 pixels were used to read out the fluorescence intensity profile of individual active zones. At least 30 active zones per ROI and larva were analyzed. For plotting the data and statistical calculations, we used Igor Pro 8 and GraphPad Prism 10.2.3.

Immunohistochemistry

For immunohistochemistry, L3 larvae were dissected as described above and the VNC along with the motor nerves were removed. The specimen was then fixed for 7 minutes in ice cold (-30°C) 100% ethanol. For this, the saline was replaced by ice cold ethanol and rinsed a few times to assure cooling down of the specimen. Then the preparation was kept in the freezer at -30°C for 7minutes. Afterwards, the specimen was treated with PBS 0.1M with 0.3 % TritonX (PBS-Tx) at room temperature for 3x10 minutes, rocking.

Ca_v2^{sfGFP} (Gratz et al. 2019) localization (Figs. 2 and 3): Primary antibodies (α-brp nc-82, 1:400, DSHB; α-HRP rabbit, 1:500, Jackson Immunoresearch Cat# 323-005-021) were applied in PBS-Tx 0.3 % overnight at 4°C, rocking. Next day, primary antibody solution was removed, the preparation rinsed a few times with PBS-Tx 0.3 % and then washed 3x10 minutes with PBS-Tx 0.3 % at room temperature, rocking. 2 hour application of α-GFP nanobody (Fluotag X4 α-GFP Alexa 647, Nanotag Biotechnologies, Germany, Cat# N0304-AF647) and secondary antibodies donkey α-mouse Alexa 555 (Jackson Immunoresearch, Cat# 715-165-151) and donkey α-rabbit Alexa 488 (Jackson Immunoresearch, Cat# 711-545-152), all at a concentration of 1:500 at room temperature.

Assessment of ΔI-IIA and ΔI-IIB channel expression: Primary antibodies (α-brp nc-82, 1:400, DSHB; α-mEOS rabbit, 1:500, Badrilla, Cat# A010-mEOS2) were applied in PBS-Tx 0.3 % overnight at 4°C, rocking. Next day, primary antibody solution was removed, the preparation rinsed a few times with PBS-Tx 0.3 % and then washed 3x10 minutes with PBS-Tx 0.3 % at room temperature, rocking. 2 hour application of α-GFP nanobody (Fluotag X4 α-GFP Abberior Star Red, Nanotag Biotechnologies, Germany, Cat# N0304-ABRED) and secondary antibodies donkey α-mouse Alexa 555 (Jackson Immunoresearch, Cat# 715-165-151) and donkey α-rabbit Alexa 488 (Jackson Immunoresearch, Cat# 711-545-152), all at a concentration of 1:500 at room temperature.

Preparations were covered to prevent bleaching of fluorophores. Then, antibodies were removed, the preparations were rinsed a few times, which was followed by 3x10 minutes PBS (no Tx). Then an ascending ethanol series with 10 minues each with 50, 70, 90, 100 % ethanol was applied at room temperature, rocking. Preparations were then mounted in methylsalicylate, covered with a high precision cover slip that was sealed with clear nail polish. Preparations were kept in the dark until

scanning with a Leica TSC SP8 upright confocal laser scanning microscope with a 40x oil NA 1.3 oil lens. Overviews were scanned without zoom at 1 µm z-step size. Magnifications were scanned with a 3.5 zoom with z-steps of 0.3 µm. All scans were done with a 3x line average.

Assessment of fluorescence intensity

For fluorescence intensity measurement of sfGFP tagged Cav2 channels in larval active zones, immunohistochemical labeling was carried out as for localization of Cav2 channels. The only difference was that each round contained animals of all genotypes that were assessed. Animals were treated in the identical dish at the same time to ensure identical treatment. Confocal images were acquired with identical settings (lasers, detectors, scanning speed).

Fluorescence intensity was compared between genotypes by employing a custom Python script (available at doi://10.5281/zenodo.11299005) in which we used brp labeling (nc-82 antibody, DSHB) as a mask and asked for Ca_v2 intensity within this mask. Intensity was then normalized to control.

Colocalization of Ca_v2 and brp scaffold protein

To determine the Pearson correlation coefficient and the Manders co-occurrence coefficients of Cav2 and brp stainings using the Costes' threshold calculation (Manders et al. 1993; Costes et al. 2004) a custom Python script was utilized (available at doi://10.5281/zenodo.11299005).

In image stacks triple stained for Cav2, brp and HRP that had been deconvolved with the software Huygens, HRP staining served as a mask in which the desired coefficients were calculated for Cav2 and brp.

Super resolution microscopy (STED) and deconvolution

STED images were acquired at a Leica Stellaris 8 STED system (*Leica microsystems*) equipped with a pulsed white light laser (WLL) for excitation ranging from 440 to 790 nm and a 775 nm pulsed laser for depletion. Samples were imaged with a 93x glycerol objective (*Leica,* HC APO 93x/1.30 GLYC motCORR). For excitation of the respective channels the WLL was set to 640 nm for FluoTag-X4 anti-GFP Atto647N (NanoTag Biotechnologies, Cat# N0304-At647N) or 580 nm for Abberior Star 580 conjugated FluoTag-X2 anti-mouse antibody (NanoTag Biotechnologies, Cat# N2702-Ab580). Emission were detected in between 650-710 nm for Atto647N and in between 590-640 nm for Abberior Star 580. STED was attained by using the 775 nm laser for both channels. Additionally a 3rd confocal channel was acquired (HRP, not shown, labeled with rabbit α-HRP antibody, Jackson Immunoresearch Cat# 323-005-021) by using 488 nm light for excitation of Alexa488 (Jackson Immunoresearch, Cat# 711-545-152) and an emission band of 500 – 530nm. Scanning properties were set to a format of 1024x1024 pixels, optical zoom factor to 5 (x/y=24.44 nm, z=191.69 nm) and scanning speed to 400 lines per second. Detectors were operated in in photon counting mode for both channels by 3 times line accumulation. For $_{gated}$STED, detector time gates were set to 0.5-6 ns for both channels.

Deconvolution of STED stacks was done with Huygens Essential (*Scientific Volume Imaging, The Netherlands, http://svi.nl*). Within the *Deconvolution wizard*, images were subjected to background correction. *Signal-to-noise ratio* was set to 20*. The Optimized iteration mode of the CMLE* was applied by using 40 Iterations.

Behavioral experiments

Wandering L3 larvae were selected off vial walls for crawling experiments and starved in empty vials for 5 minutes. Afterwards, they were placed in the middle of a plasticine square on an agarose gel (1% in H2O dest) using a brush. This square itself was placed on a tracking table with an acrylic glass plate. Usually, 10 larvae of the same genotype were recorded at a time. Occasionally, less than 10 larvae were available, in which case fewer larvae were rec-orded. Dishes were freshly poured each day before starting experiments. To prevent the lar-vae from escaping the boundary, an electrically charged wire was placed inside the square boundaries. Crawling pictures were obtained with a camera (Basler acA2040-90µm) from below the glass plate at a frame rate of 4 Hz for 5 minutes via pylon viewer (Version 6). Since few larvae were able to dig into the gel through small holes, only larvae that stayed inside the arena for 5 minutes were included into analysis. Tracking data of larval crawling were analyzed via the free software FIMtrack (University of Münster, Germany). Parameters that were read out included (but were not limited to) number of stops, average and maximum speed. The full list of data that were read out is available (doi://10.5281/zenodo.11299005). For explanation of read-out parameters, consult the FIMtrack manual (University of Münster website).

Statistics and figure generation

Statistical analysis was performed with GraphPad Prism 10.2.1 (395). Data were tested for normal distribution using the Shapiro Wilk test. Normally distributed data were compared using either Student's T-test (for two groups) or one-way ANOVA (for more than two groups) with subsequent Sidak's Test post-hoc test for multiple comparisons or Dunnett's test for each test group against control (planned comparisons). For non-normally distributed data either Mann-Whitney U-test (for two groups) or Kruskal Wallis Anova (with more than two groups) with subsequent Dunn's post-hoc test for multiple comparisons or for test groups against control (planned comparisons) were used.

Differences were considered significant if $p \leq 0.05$ *, $p \leq 0.01$ **, $p \leq 0.001$ ***, $P \leq 0.0001$ ****.

Diagrams were generated with GraphPad Prism 10.2.1 (395) or Microsoft Excel 365. Figures with immunohistochemical images were generated with LasX software (Leica Microsystems, Wetzlar, Germany), with Fiji (www.Fiji.sc), or with Amira (version 6.5, Thermo Scientific). Images and diagrams were imported into CorelDraw Graphics Suite 2022 (Corel Corporation) either as Tiff images or as enhanced meta files (.emf) for figure production. Final figures were exported as .tif files.

All data and script is available at doi://10.5281/zenodo.11383963. Cacophony exon out flies will be sent to the Drosophila Bloomington Stock Center upon publication.

Acknowledgments

We thank Kerstin Birod for performing Western Blots, Kate O'Connor-Giles for providing cacophony^{mEOS4b} flies, Tayfun Göncü for participating in gathering STED data, Susanne Hornig for confocal recordings of co-expressed cacophony exon out variants. This work was supported by a DFG research grant to S. Ryglewski (RY117/3-2).

References

Atwood HL, Karunanithi S (2002) Diversification of synaptic strength: Presynaptic elements. Nat. Rev. Neurosci. 3, 497–516.

Blanchette M, Green RE, Brenner SE, Rio DC (2005) Global analysis of positive and negative pre-mRNA splicing regulators in Drosophila. Genes Dev 19(11):1306-14.

Brooks AN, Aspden JL, Podgornaia AI, Rio DC, Brenner SE (2011) Identification and experimental validation of splicing regulatory elements in Drosophila melanogaster reveals functionally conserved splicing enhancers in metazoans. RNA 17(10):1884-94.

Costes S, Daelemans D, Cho EH, Dobbin Z, Pavlakis G, Lockett S (2004) Automatic and quantitative measurement of protein-protein colocalization in live cells. Biophysical Journal, 86(6), 3993–4003.

Davis GW, Müller M (2015) Homeostatic control of presynaptic neurotransmitter release. Annu Rev Physiol 77:251-70.

Dietrich D, Kirschstein T, Kukley M, Pereverzev A, von der Brelie C, Schneider T, et al. (2003) Functional specialization of presynaptic $Ca_v2.3$ Ca2+ channels. Neuron 39:483–496.

Dittman JS, Ryan TA (2019) The control of release probability at nerve terminals. Nat Rev Neurosci 20(3):177-186.

Dolphin AC (2009) Calcium channel diversity: multiple roles of calcium channel subunits. Curr Opin Neurobiol 19(3):237-44.

Dolphin AC, Lee A (2020) Presynaptic calcium channels: specialized control of synaptic neurotransmitter release. Nat Rev Neurosci 21(4):213-229.

Doudna JA, Charpentier E (2014) Genome editing. The new frontier of genome engineering with CRISPR-Cas9. Science 346(6213):1258096.

Eggermann E, Bucurenciu I, Goswami SP, Jonas P (2011) Nanodomain coupling between Ca^{2+} channels and sensors of exocytosis at fast mammalian synapses. Nat Rev Neurosci 13(1):7-21.

Emperador-Melero J, Kaeser PS (2020) Assembly of the presynaptic active zone. Curr Opin Neurobiol 63:95-103.

Fioravante D, Regehr WG (2011) Short-term forms of presynaptic plasticity. Curr Opin Neurobiol 21(2):269-74.

Ghelani T, Escher M, Thomas U, Esch K, Lützkendorf J, Depner H, Maglione M, Parutto P, Gratz S, Matkovic-Rachid T, Ryglewski S, Walter AM, Holcman D, O'Connor Giles K, Heine M, Sigrist SJ (2023) Interactive nanocluster compaction of the ELKS scaffold and Cacophony Ca2+ channels drives sustained active zone potentiation. Sci Adv 9(7):eade7804.

Gratz SJ, Ukken FP, Rubinstein CD, Thiede G, Donohue LK, Cummings AM, O'Connor-Giles KM (2014) Highly specific and efficient CRISPR/Cas9-catalyzed homology-directed repair in Drosophila. Genetics 196(4):961-71.

Gratz SJ, Goel P, Bruckner JJ, Hernandez RX, Khateeb K, Macleod GT, Dickman D, O'Connor-Giles KM (2019) Endogenous Tagging Reveals Differential Regulation of Ca2+ Channels at Single Active Zones during Presynaptic Homeostatic Potentiation and Depression. J Neurosci 39(13):2416-2429.

Guerrero G, Reiff DF, Agarwal G, Ball RW, Borst A, Goodman CS, Isacoff EY (2005) Heterogeneity in synaptic transmission along a Drosophila larval motor axon. Nat Neurosci 8(9):1188-96.

Guo Y, Wang Y, Zhang W, Meltzer S, Zanini D, Yu Y, Li J, Cheng T, Guo Z, Wang Q, Jacobs JS, Sharma Y, Eberl DF, Göpfert MC, Jan LY, Jan YN, Wang Z (2016) Transmembrane channel-like (tmc) gene regulates Drosophila larval locomotion. PNAS 113(26):7243-8.

Harris KP, Littleton JT (2015) Transmission, Development, and Plasticity of Synapses. Genetics 201, 345–375.

Heck J, Parutto P, Ciuraszkiewicz A, Bikbaev A, Freund R, Mitlöhner J, Andres-Alonso M, Fejtova A, Holcman D, Heine M (2019) Transient Confinement of CaV2.1 Ca2+-Channel Splice Variants Shapes Synaptic Short-Term Plasticity. Neuron 103(1):66-79.e12.

James TD, Zwiefelhofer DJ, Frank CA (2019) Maintenance of homeostatic plasticity at the Drosophila neuromuscular synapse requires continuous IP3-directed signaling. Elife 8:e39643.

Jia XX, Gorczyca M, Budnik V (1993) Ultrastructure of neuromuscular junctions in Drosophila: comparison of wild type and mutants with increased excitability. J Neurobiol 24(8):1025-1044.

Kadas D, Klein A, Krick N, Worrell JW, Ryglewski S, Duch C (2017) Dendritic and Axonal L-Type Calcium Channels Cooperate to Enhance Motoneuron Firing Output during Drosophila Larval Locomotion. J Neurosci 37(45):10971-10982.

Kawasaki F, Collins SC, Ordway RW (2002) Synaptic calcium-channel function in Drosophila: analysis and transformation rescue of temperature-sensitive paralytic and lethal mutations of cacophony. J Neurosci 22(14):5856-64.

Kawasaki F, Zou B, Xu X, Ordway RW (2004) Active zone localization of presynaptic calcium channels encoded by the cacophony locus of Drosophila. J Neurosci 24(1):282-5.

Kittel RJ, Wichmann C, Rasse TM, Fouquet W, Schmidt M, Schmid A, Wagh DA, Pawlu C, Kellner RR, Willig KI, Hell SW, Buchner E, Heckmann M, Sigrist SJ (2006) Bruchpilot promotes active zone assembly, Ca2+ channel clustering, and vesicle release. Science 312(5776):1051-4.

Krick N, Ryglewski S, Pichler A, Bikbaev A, Götz T, Kobler O, Heine M, Thomas U, Duch C (2021) PNAS 118(28):e2106621118.

Laine RF, Tosheva KL, Gustafsson N, Gray RDM, Almada P, Albrecht D, Risa GT, Hurtig F, Lindås AC, Baum B, Mercer J, Leterrier C, Pereira PM, Culley S, Henriques R (2019) NanoJ: a high-performance open-source super-resolution microscopy toolbox. J Phys D Appl Phys 52(16):163001.

Li L, Bischofberger J, Berger J (2007) Differential gating and recruitment of P/Q-, N-, and R-type Ca2+ channels in hippocampal mossy fiber boutons. J Neurosci 27(49):13420-13429.

Liu Y, Hasegawa E, Nose A, Zwart MF, Kohsaja H (2023) Synchronous multi-segmental activity between metachronal waves controls locomotion speed in Drosophila larvae. Elife 12:e83328.

Manders EMM, Verbeek FJ, Aten JA (1993) Measurement of co-localization of objects in dual-colour confocal images. Journal of Microscopy 169(3):375-382.

Moser T, Karagulyan N, Neef J, Jaime Tobón LM (2023) Diversity matters - extending sound intensity coding by inner hair cells via heterogeneous synapses. EMBO 42(23):e114587

Moser T, Grabner CP, Schmitz F (2020) Sensory Processing at Ribbon Synapses in the Retina and the Cochlea. Physiol Rev 100(1):103-144.

Newman ZL, Bakshinskaya D, Schultz R, Kenny SJ, Moon S, Aghi K, Stanley C, Marnani N, Li R, Bleier J, Xu K, Isacoff EY (2022) Determinants of synapse diversity revealed by super-resolution quantal transmission and active zone imaging. Nat Comm 13(1):229.

Nicoll RA, Schmitz D (2005) Synaptic plasticity at hippocampal mossy fibre synapses. Nat Rev Neurosci 6(11):863-76.

Rebola N, Reva M, Kirizs T, Szoboszlay M, Lőrincz A, Moneron G, Nusser Z, DiGregorio DA (2019) Distinct Nanoscale Calcium Channel and Synaptic Vesicle Topographies Contribute to the Diversity of Synaptic Function. Neuron 104(4):693-710.

Ryglewski S, Lance K, Levine RB, Duch C (2012) Ca(v)2 channels mediate low and high voltage-activated calcium currents in Drosophila motoneurons. J Physiol 590(4):809-25.

Ryglewski S, Kilo L, Duch C (2014) Sequential acquisition of cacophony calcium currents, sodium channels and voltage-dependent potassium currents affects spike shape and dendrite growth during postembryonic maturation of an identified Drosophila motoneuron. Eur J Neurosci 39(10):1572-85.

Ryglewski S, Kadas D, Hutchinson K, Schuetzler N, Vonhoff F, Duch C (2014) Dendrites are dispensable for basic motoneuron function but essential for fine tuning of behavior. PNAS 111(50):18049-54.

Sanyal S (2009) Genomic mapping and expression patterns of C380, OK6 and D42 enhancer trap lines in the larval nervous system of Drosophila. Gene Expr Patterns 9(5):371-80.

Sheng J, He L, Zheng H, Xue L, Luo F, Shin W, et al. (2012) Calcium-channel number critically influences synaptic strength and plasticity at the active zone. Nat. Neurosci. 15:998–1006.

Smith LA, Peixoto AA, Kramer EM, Villella A, Hall JC (1998) Courtship and visual defects of cacophony mutants reveal functional complexity of a calcium-channel alpha1 subunit in Drosophila. Genetics 149(3): 1407-1426.

Smith LA, Wang X, Peixoto AA, Neumann EK, Hall LM, Hall JC (1996) A Drosophila calcium channel alpha1 subunit gene maps to a genetic locus associated with behavioral and visual defects. J Neurosci 16(24): 7868-7879.

Sternberg SH, Doudna JA (2015) Expanding the Biologist's Toolkit with CRISPR-Cas9. Mol Cell 58(4):568-74.

Südhof TC (2012) Calcium control of neurotransmitter release. Cold Spring Harb Perspect Biol 4(1):a011353.

Südhof TC (2013) Neurotransmitter release: the last millisecond in the life of a synaptic vesicle. Neuron 80(3):675-90.

Südhof TC (2014) The molecular machinery of neurotransmitter release (Nobel lecture). Angew Chem Int Ed Engl 53(47):12696-717.

Takahashi T, Momiyama A (1993) Different types of calcium channels mediate central synaptic transmission. Nature 366:156–158.

Turrigiano GG (2008) The self-tuning neuron: synaptic scaling of excitatory synapses. Cell 135(3):422-35.

Van Vactor D, Sigrist SJ (2017) Presynaptic morphogenesis, active zone organization and structural plasticity in Drosophila. Curr Opin Neurobiol 43:119-129.

Wheeler DB, Randall A, Tsien RW (1994) Roles of N-type and Q-type Ca2+ channels in supporting hippocampal synaptic transmission. Science 264:107–111.

Wang JW, Sylwester AW, Reed D, Wu DA, Soll DR, Wu CF (1997) Morphometric Description of the Wandering Behavior in Drosophila Larvae: Aberrant Locomotion in Na+ and K+ Channel Mutants Revealed by Computer-Assisted Motion Analysis. J Neurogenet 11(3-4):231-54.

Worrell JW, Levine RB (2008) Characterization of voltage-dependent Ca2+ currents in identified Drosophila motoneurons in situ. J Neurophysiol 100(2):868-78.

Wu LG, Borst JG, Sakmann B (1998) R-type Ca2+ currents evoke transmitter release at a rat central synapse. PNAS 95:4720–4725.

Zhang W, Jiang HH, Luo F (2022) Diverse organization of voltage-gated calcium channels at presynaptic active zones. Front Synaptic Neurosci 14:1023256.

Figures and Legends

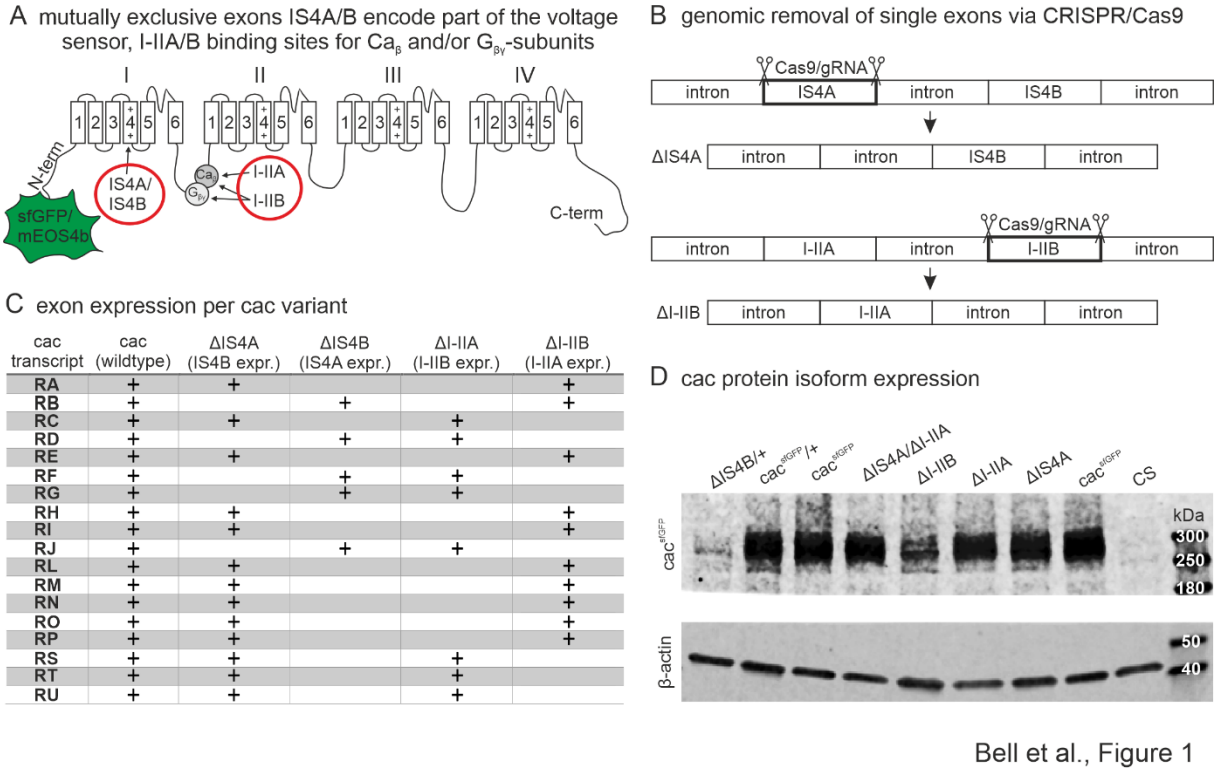

cac transcript	cac (wildtype)	ΔIS4A (IS4B expr.)	ΔIS4B (IS4A expr.)	ΔI-IIA (I-IIB expr.)	ΔI-IIB (I-IIA expr.)
RA	+	+			+
RB	+		+		+
RC	+	+		+	
RD	+		+	+	
RE	+	+			+
RF	+		+	+	
RG	+		+	+	
RH	+	+			+
RI	+	+			+
RJ	+		+	+	
RL	+	+			+
RM	+	+			+
RN	+	+			+
RO	+	+			+
RP	+	+			+
RS	+	+		+	
RT	+	+		+	
RU	+	+		+	

Figure 1. *Cacophony alternative splicing gives rise to different protein isoforms.* **(A)** Schematic of cacophony with N-terminal sfGFP or mEOS4b tag and two exon pairs that are spliced mutually exclusively. *IS4A* and *IS4B* exons encode isoforms of the 4th transmembrane domain (S4) and thus part of the voltage sensor of the first homologous repeat (I) of the calcium channel, while *I-IIA* and *I-IIB* give rise to two versions of the intracellular linker between homologous repeats I and II. I-IIA contains a non-well conserved binding site for voltage gated calcium channel β-subunits (Ca_{β}) whereas I-IIB gives rise to a conserved Ca_{β}-binding site as well as a binding site for G-protein βγ-subunits ($G_{\beta\gamma}$). **(B)** Genomic removal of one of the mutually exclusively spliced exons of one or two exon pairs by CRISPR/Cas9 mediated double strand breaks in the germ line results in exon out mutants by imprecise excision of the cut exons and cell-intrinsic DNA repair. **(C)** *Cacophony* gives rise to 18 annotated transcripts (RA-RU, left). Multiple variants express the same mutually exclusive exons but differ with respect to expression of other alternatively spliced but not mutually exclusive exons. Removal of the mutually exclusive exons *IS4A/IS4B* and/or *I-IIA/I-IIB* allows expression of fewer *cacophony* splice variants. Transcript variants that are possible upon exon excision are marked by +. **(D)** Western Blots reveal expression of GFP-tagged cacophony protein (cac^{sfGFP}) for all excision variants at the expected band size of ~240 kDa (cacophony) plus ~30 kDa (sfGFP, top), while no band can be detected in the Canton S wildtype (CS, top, right) that does not express cac^{sfGFP}. 10 adult brains were used of hemizygous males for all genotypes except for *ΔIS4B* which is homo-/hemizygous lethal. For *ΔIS4B* 20 brains of heterozygous females and a heterozygous cac^{sfGFP} control were used (F1 females from cross with Canton S wildtype flies(+)). β-actin was used as loading control (bottom). *ΔIS4B* shows weak expression (top, left), while all other exon out variants express strongly, although *ΔI-IIB* shows somewhat weaker expression (top, middle).

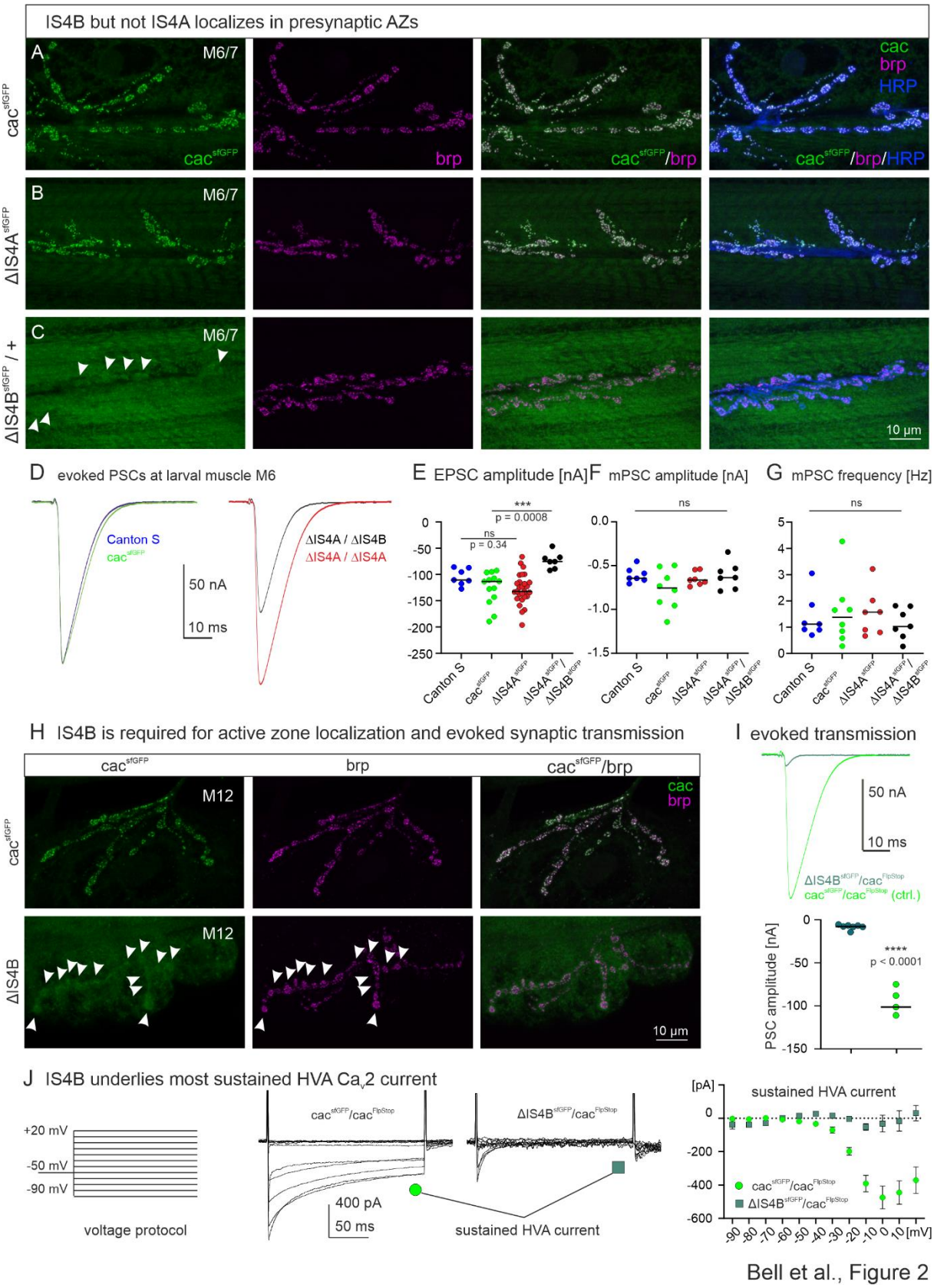

Figure 2. *The IS4B exon is required for Ca_v2 localization to active zone and for evoked synaptic transmission.* **(A-C)** Representative confocal projection views of triple labels for GFP tagged Ca_v2 channels (green), the active zone marker brp (magenta), and HRP to label axonal membrane (blue) in control animals with all Ca_v2 exons (cac^{sfGFP}, top row, **A**), in animals with selective excision of either the

alternative exon *IS4A* (*ΔIS4A*^{sfGFP}, middle row, **B**), or the alternative exon *IS4B* (*ΔISAB*^{sfGFP}, bottom row, **C**). Excision of *IS4B* is embryonic lethal, so that localization analysis was conducted in heterozygous animals (*ΔISAB*^{sfGFP}*/+*). The gross morphology of the neuromuscular junctions (muscle fibers, bouton numbers and sizes, active zone numbers) was similar in all three genotypes. GFP tagged Ca_v2 channels localize to active zones **(A)** as previously reported (Gratz et al. 2019; Krick et al. 2021). Excision of the *IS4A* exon does neither impact Ca_v2 channel active zone localization nor labeling intensity **(B)**. By contrast, upon excision of the *IS4B* exon, Ca_v2 channel label (white arrowheads) is faint and not strictly co-localized with active zones **(C)**. **(D, E)** Representative traces of evoked synaptic transmission as recorded in TEVC from muscle fiber 6 upon extracellular stimulation of the motor nerve from a wildtype control animal (CS, blue), an animal with GFP tagged Ca_v2 channels (cac^{sfGFP}, green), and animals with GFP tagged Ca_v2 channels and either *IS4A* exon excision (*ΔISA4*, orange) or *IS4B* excision (*ΔISAB*, transheterozygous over *ΔISA4*, black trace). **(D)** Postsynaptic currents (PSCs) are similarly shaped between CS control (blue) and animals with GFP-tagged Ca_v2 channels (cac^{sfGFP}, green), and **(E)** PSC amplitudes are not statistically different (p=0.34, two sided Tukey's multiple comparison test). In animals with homozygous *IS4A* exon excision (orange), PSC amplitude is slightly but not significantly increased (p=0.18, two sided Tukey's multiple comparison test). In transheterozygous animals with *IS4A* excision on one chromosome and *IS4B* excision on the other one, PSC amplitude is significantly decreased (p=0.0008), two sided Tukey's multiple comparison test). **(F)** Quantal size (mPSC amplitude) and spontaneous release frequency **(G)** show no significant difference between genotypes. **(H, I)** Since animals homozygous for *IS4B* exon excision are lethal, we created mosaic animals that were heterozygous for Ca_v2 in most neurons but hemizygous for either cac^{sfGFP} or *ΔISAB* in motoneurons innervating muscle M12 (see methods, *cac*^{FlpStop}). In control with all Ca_v2 exons (cac^{sfGFP}, green, top row) cac^{sfGFP} colocalizes with brp (magenta) in presynaptic active zones on M12 **(H)** and evoked synaptic transmission induces PSCs of about 100 nA amplitude **(I)**. By contrast, upon deletion of *IS4B* (**H**, bottom row) in motoneurons to M12 fuzzy Ca_v2 label is found throughout the motor terminals, but Ca_v2 (green) does not strictly colocalize with brp (magenta) in active zones **(H)** and evoked synaptic transmission is reduced by more than 90%, Student's T-test, $p < 0.0001$ **(I)**. **(J)** HVA Ca_v2 currents as recorded from the somata of adult flight motoneurons in mosaic animals with only one copy of the Ca_v2 locus in flight motoneurons (see methods). HVA currents are measured by starting from a holding potential of -50 mV (LVA inactivation) followed by step command voltages from -90 mV to +20 mV in 10 mV increments (left). In GFP-tagged controls (*cac*^{sfGFP} / *cac*^{FlpStop}) this reveals transient and sustained HVA current components. By contrast, following excision of the *IS4B* exon (*ΔISAB*^{sfGFP} / *cac*^{FlpStop}), the sustained HVA current is nearly absent. Current-voltage (IV) relation of sustained HVA for controls with all Ca_v2 exons (cac^{sfGFP}, green circles, n = 8) and following excision of *IS4B* (*ΔIS4B*^{sfGFP}, dark green squares, n = 4).

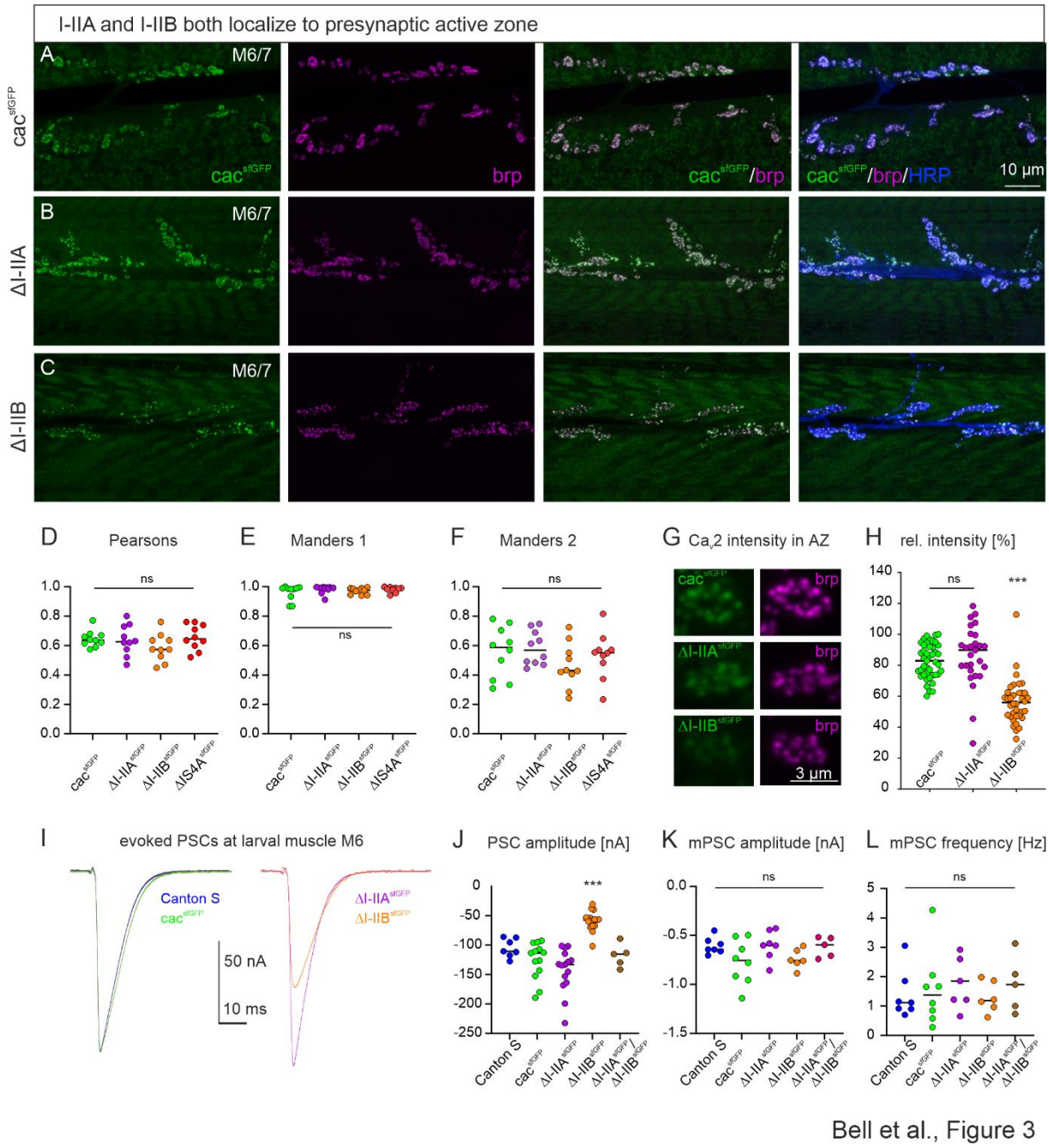

Figure 3. *The I-II exon does not affect active zone localization but release probability.* **(A-C)** Representative confocal projection views of triple labels for GFP tagged Ca_v2 channels (green), the active zone marker brp (magenta), and HRP to label axonal membrane (blue) in control animals with all Ca_v2 exons (cac^{sfGFP}, top row, **A**), with selective excision of either the alternative exon *I-IIA* (*I-IIA*^{sfGFP}, middle row, **B**), or the alternative exon *I-IIB* (*I-IIB*^{sfGFP}, bottom row, **C**). The gross morphology of the neuromuscular junctions (muscle fibers, bouton numbers and sizes, active zone numbers) was similar in all three genotypes (not shown). Excision of the *I-IIA* exon does neither impact Ca_v2 channel active zone localization nor labeling intensity **(B)**. Excision of *I-IIB* does not impact Ca_v2 channel active zone localization but labeling intensity seems lower **(C)**. **(D-F)** Quantification of Ca_v2 channel co-localization with the active zone marker brp yields a similar Pearson's colocalization coefficient **(D)** as well as similar Manders 1 **(E)** and Manders 2 **(F)** coefficients for controls and both exon-out variants of the *I-II* locus. **(G)** *I-IIB*^{sfGFP} shows fainter immunofluorescence signals in the active zone as compared to control (cac^{sfGFP}) and *I-IIA*^{sfGFP}. **(H)** Quantification confirms a significant reduction in *I-IIB*^{sfGFP} labeling intensity

(Kruskal Wallis ANOVA with Dunn's post hoc test, $p < 0.0001$) and no differences between Δ*I-IIA*^{sfGFP} and control ($p > 0.99$). **(I)** Evoked synaptic transmission as recorded in TEVC from muscle fiber 6 upon extracellular stimulation of the motor nerve. Postsynaptic currents (PSCs) are of similar shape and amplitude for CS control (blue) and animals with GFP-tagged Ca_v2 channels (cac^{sfGFP}, green, p=0.34, two sided Tukey's multiple comparison test). Excision of *I-IIA* (Δ*I-IIA*^{sfGFP}, magenta) has no effect on evoked release amplitude (p=0.52, two sided Tukey's multiple comparison test), but excision of *I-IIB* (Δ*I-IIB*^{sfGFP}, orange) reduces evoked release significantly ($p < 0.0001$). **(J)** Quantification of PSC amplitude reveals a highly significant reduction in Δ*I-IIB*^{sfGFP} (orange) as compared cac^{sfGFP} controls (green), but neither animals with excision of the *I-IIA* exon (magenta), nor transheterozygous animals with excision of *I-IIA* on one and *I-IIB* on the chromosome (brown) show differences to control (p=0.97, two sided Tukey's multiple comparison test). **(K)** Quantal size (mPSC amplitude) and spontaneous release frequency **(L)** show no significant difference among genotypes.

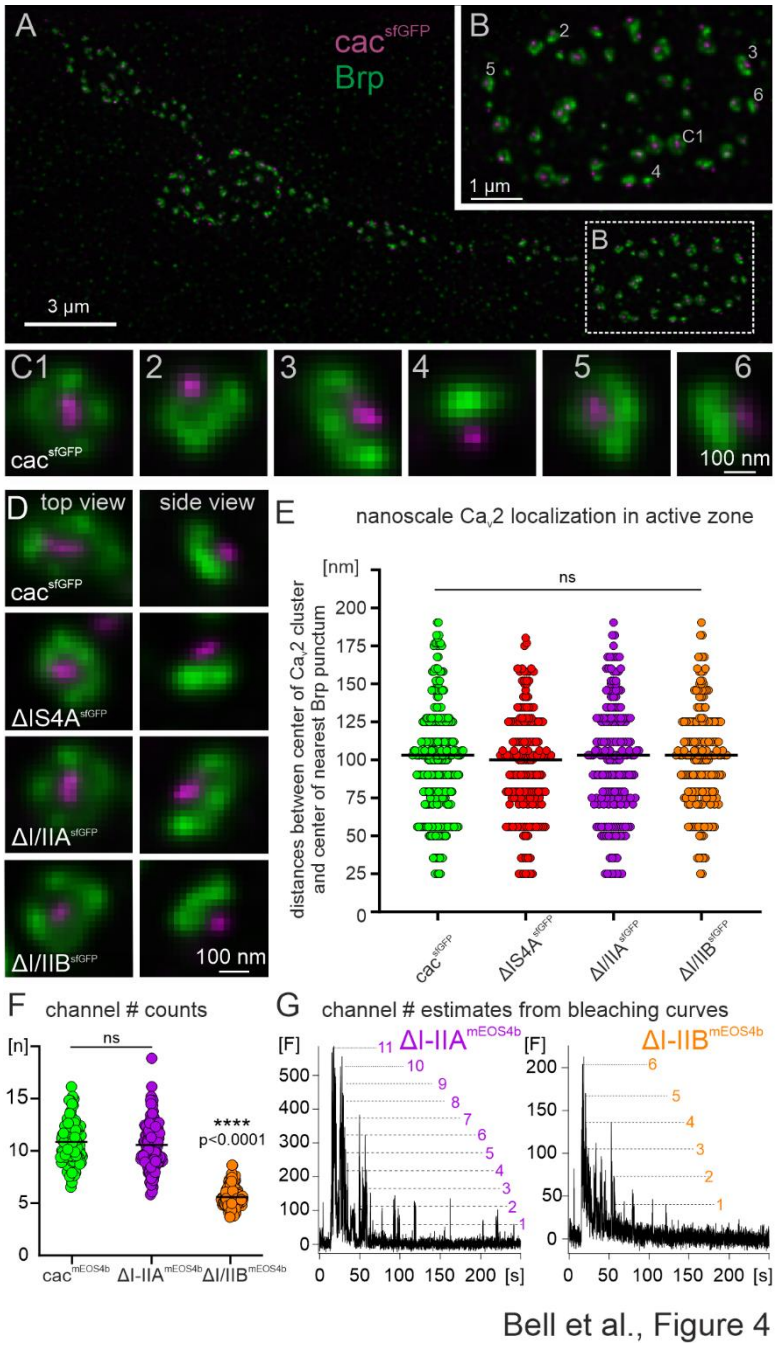

Figure 4. *Dual color STED* imaging reveals *equal nanoscale channel localization in AZs of Ca_v2 for all exon-out variants, and live sptPALM imaging reduced channel numbers in AZs for ΔI-IIB.* **(A)** Representative intensity projection image of the active zone marker bruchpilot (labeled with anti-brp, green) and Ca_v2 clusters (cac^{sfGFP} labeled with anti-GFP, magenta) as imaged with dual color STED at motoneuron axon terminal boutons on larval muscle M6. The dotted white box demarks one bouton that is enlarged in **(B)**. Each Ca_v2 cluster (magenta) is in close spatial proximity to the active zone marker brp (green). In 3D STED the active zone Ca_v2 -brp is viewed from different angles. Top views (see C1 in B and in selective enlargement) show 4 brp puncta that symmetrically surround the central Ca_v2 cluster. Viewing active zones at the edge of the bouton shows the Ca_v2 cluster facing to the outside and the brp puncta in close proximity (see 2-6). **(C)** Selective enlargements of each active zone that is numbered in B. **(D)** Top views (left column) and side views (right column) of the Ca_v2-brp arrangement in active zones in controls with GFP-tagged Ca_v2 channels, (cac^{sfGFP}, top row), with excision of exon *IS4A*

(⍰*ISA4*^{sfGFP}, second row), with excision of exon *I/IIA* (⍰*I/IIA*^{sfGFP}, third row), and with excision of exon *I/IIB* (⍰*I/IIB*^{sfGFP}, bottom row). **(E)** Quantification of the distances between the center of each Ca_v2 punctum to the nearest brp punctum in the same focal plane. **(F-G)** Live sptPALM imaging of mEOS4b tagged Ca_v2 channels from AZs of MN terminals on muscle 6 in controls with full isoform diversity (cac^{mEOS4b,} green) and following the removal of either *I-IIA* (*ΔI-IIA*^{mEOS4b}, purple) or *I-IIB* (*ΔI-IIB*^{mEOS4b}, orange). **(F)** Quantification of channel numbers from bleaching curves **(G)** reveals ~ 9-11 Ca_v2 channels per AZ for tagged controls, which matches previous reports (Ghelani et al. 2023). Counts for *ΔI-IIA* reveal no significant differences (Kruskal-Wallis test with Dunn's posthoc comparison, p=0.94), but Ca_v2 channel number in AZs is reduced by ~50 % in *ΔI-IIB* ($p<0.0001$). **(G)** Bleaching curves of single active zones were illuminated after ~10 s and then imaged under constant illumination for another 240 s. Discrete bleaching steps (dotted lines) indicate the bleaching of single mEOS4b tagged Ca_v2 channels. Comparing the amplitudes of single events and their integer multiples (dotted lines) to the maximum fluorescence at illumination start allows estimates of the total channel number per AZ.

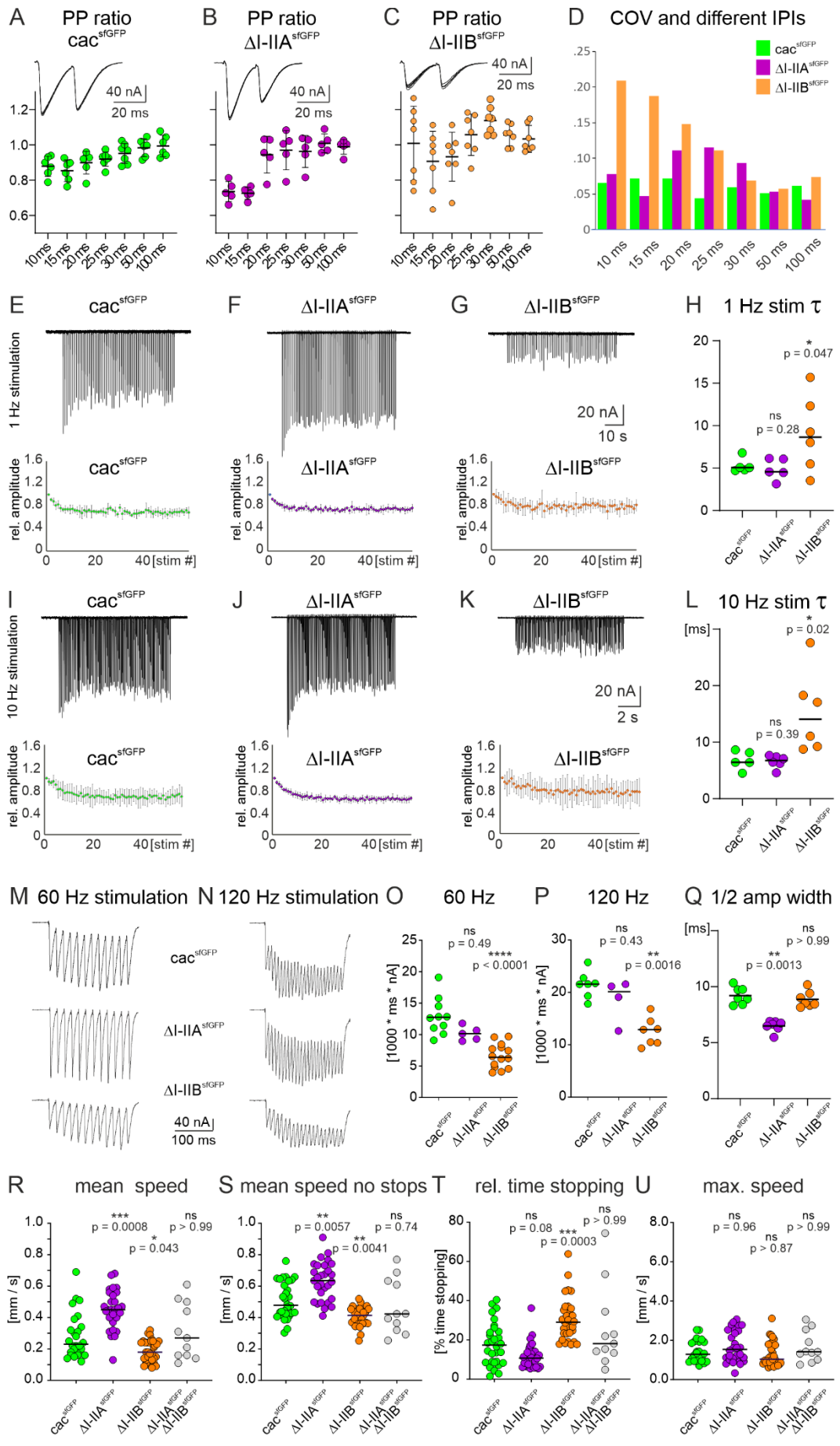

Bell et al., Figure 5

- **Figure 5.** *Alternative splicing in the I-II linker affects short term plasticity and motor behavior.* **(A-B)** Paired pulse ratio (PPR, ratio of second PSC divided by first PSC amplitude) as measured in 0.5 mM external calcium at different interpulse intervals (IPSs ranging from 10 ms to 100 ms) in control animals with GFP-tagged Ca_v2 (cac^{sfGFP}, **A**), in animals with removal of *I-IIA* (*ΔI-IIA*^{sfGFP}, **B**), and in animals with removal of *I-IIB* (*ΔI-IIB*^{sfGFP}, **C**). **(E-G)** Synaptic depression as measured in 0.5 mM external calcium in response to stimulus trains of 1 minute duration at 1 Hz frequency for animals with GFP-tagged Ca_v2 (cac^{sfGFP}, **E**), following removal of *I-IIA* (*ΔI-IIA*^{sfGFP}, **F**), and with removal of *I-IIB* (*ΔI-IIB*^{sfGFP}, **G**). The upper traces show representative TEVC recordings from the postsynaptic muscle cell, and the diagrams mean values (n=5 for E and F, N=6 for G, error bars are SD). For all 3 genotypes, depression reaches steady state at ~ 80 % of the original PSC amplitude, but upon excision of *I-IIB* it is more variable **(G)** and slower **(H)** as compared to control and *I-IIA* excision **(E, F, H)**. **(I-L)** Synaptic depression in response to stimulus trains at 10 Hz frequency for animals with GFP-tagged Ca_v2 (cac^{sfGFP}, **I**), following removal of *I-IIA* (*ΔI-IIA*^{sfGFP}, **J**), and with removal of *I-IIB* (*ΔI-IIB*^{sfGFP}, **K**). Again, depression is most variable between animals upon excision of *I-IIB* **(K, L)** and it is slower as compared to control and *ΔI-IIA* **(L)**. Motoneuron stimulation at 60 **(N)** or 100 Hz **(M)** frequency, both for durations of 200 ms in animals with GFP-tagged Ca_v2 (cac^{sfGFP}, upper traces), following removal of *I-IIA* (*ΔI-IIA*^{sfGFP}, middle traces), and with removal of *I-IIB* (*ΔI-IIB*^{sfGFP}, lower traces). To compare charge transfer during across the NMJ during high frequency bursts the total PSC area below baseline (prior to stimulation) was measured during each 200 ms burst and plotted for each genotype for 60 Hz stimulation in **(O)** and for 100 Hz stimulation in **(P). (Q)** shows single evoked PSC half amplitude width. (R-U) show different measurements during larval crawling for control animals with GFP-tagged Ca_v2 (cac^{sfGFP}), removal of *I-IIA* (*ΔI-IIA*^{sfGFP}), removal of *I-IIB* (*ΔI-IIB*^{sfGFP}), and in transheterozygous animals with removal of I-IIA on one and removal of I-IIB on the other chromosome (*ΔI-IIA*^{sfGFP}/*ΔI-IIB*^{sfGFP}). The measured parameters are mean speed during 10 minutes of crawling **(R)**, mean speed without any stops **(S)**, the relative time spent stopping **(T)** and the maximum speed reached **(U)**. In all diagrams each dot demarks a measurement from a different animal and horizontal bars the medians. For statistics, non-parametric Kruskal Wallis ANOVA with planned Dunn's posthoc comparison to control was conducted.

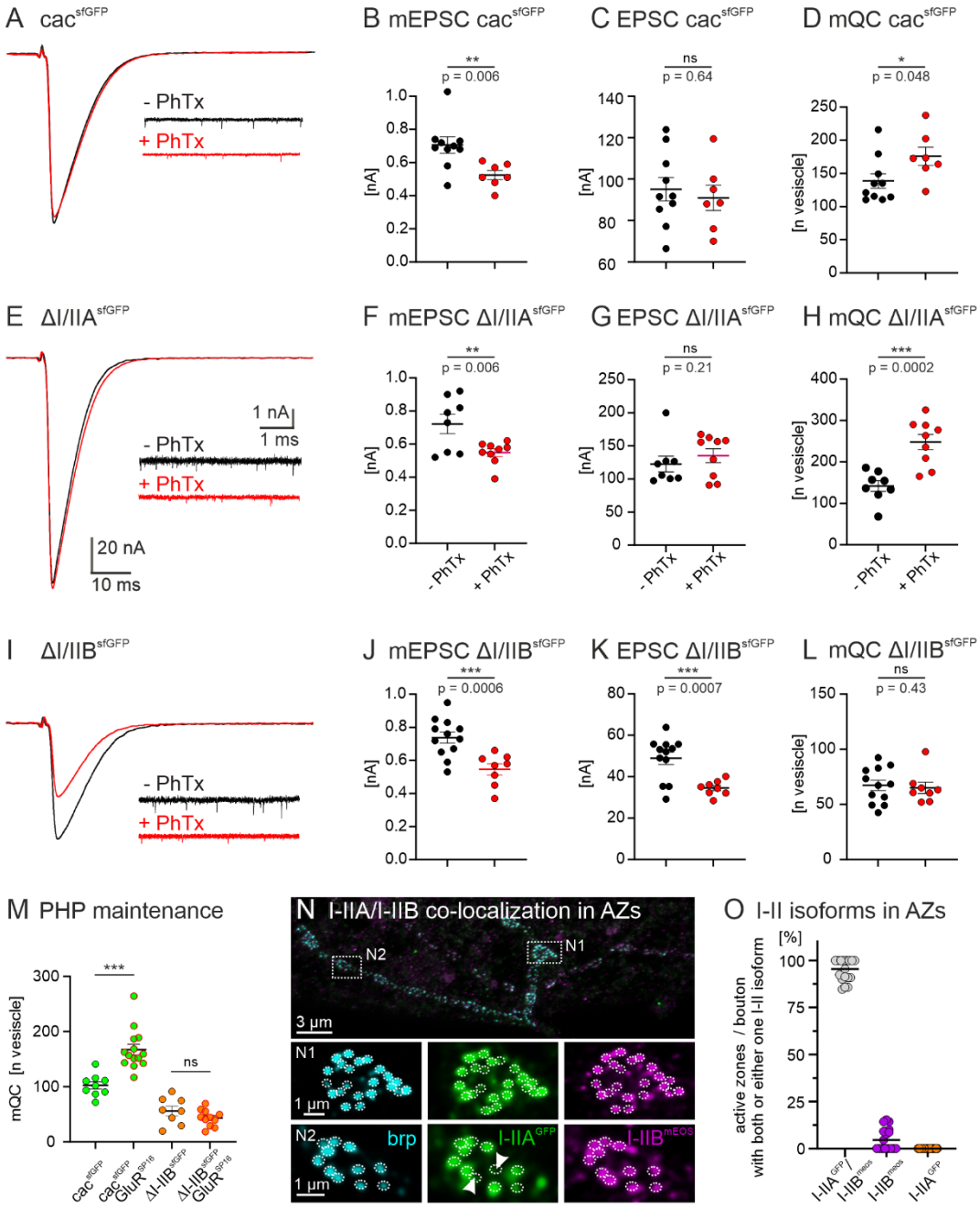

Bell et al., Figure 6

Figure 6. *Removal of I-IIB impairs presynaptic homeostatic potentiation.* **(A-D)** Presynaptic homeostatic potentiation (PHP) can be induced in control animals with GFP-tagged Ca_v2 (cac^{sfGFP}) by bath application of the glutamate IIA receptor blocker philanthotoxin (PhTx). As compared to control **(A**, black traces), bath application of PhTx **(A**, red traces) reduces the amplitude of miniature postsynaptic currents **(B**, mEPSCs) significantly, but EPSC amplitude upon evoked synaptic transmission remains unaltered **(C)** because the number of SVs that are released upon one presynaptic action potential **(D,** mean quantal content, mQC) is significantly increased to compensate for the smaller postsynaptic response to a given amount of neurotransmitter release. **(E-H)** PHP is also measured upon PhTx application to animals with removal of *I-IIA*. **(I-L)** By contrast, in animals with excision of *I-IIB* the reduction of mEPSCs by bath application of PhTx **(I** and **J)** causes a significant reduction in the amplitude of evoked synaptic

transmission (EPSC amplitude, **K)**, because no compensatory upregulation of mQC is observed **(L)**. Therefore, PHP induction requires the *I-IIB* exon. **(M)** PHP maintenance is typically assessed in *GluRIIA* mutants. PHP maintenance is observed in control animals with GFP-tagged Ca_v2 (cac^{sfGFP}) because mQC is increased in a *GluRIIA* mutant background ($GluR^{SP16}$). By contrast, in *ΔI-IIB* animals the *GluRIIA* mutant background does not cause an increase in mQC. **(N)** In animals that are transheterozygous for the removal of *I-IIA* and the removal of *I-IIB*, and carry GFP-tagged I-IIA and mEOS4b-tagged I-IIB Ca_v2, triple immunolabel for the AZ marker brp, GFP, and mEOS4b show that most active zones (cyan) contain both, GFP-tagged I-IIA (green) and mEOS4b-tagged I-IIB (magenta) channels. **(O)** Quantification shows that >95 % of all brp positive AZs contain I-IIA and I-IIB channels (gray dots), few AZs (~5 %) contain only I-IIB (magenta), and no AZ contains only I-IIA (orange).